NAVAL POSTGRADUATE SCHOOL
Monterey, California

THESIS

THE ONE-DIMENSIONALITY OF THE UPPER OCEAN MIXING AND
THE ROLE OF ADVECTION DURING THE POLE EXPERIMENT

by

Ricky Eugene Shook

September 1980

Thesis Advisor: R. W. Garwood, Jr.

Approved for public release; distribution unlimited

REPORT DOCUMENTATION PAGE		READ INSTRUCTIONS BEFORE COMPLETING FORM
1. REPORT NUMBER	2. GOVT ACCESSION NO. AD-A094 552	3. RECIPIENT'S CATALOG NUMBER
4. TITLE (and Subtitle) The One-Dimensionality of the Upper Ocean Mixing and the Role of Advection During the POLE Experiment		5. TYPE OF REPORT & PERIOD COVERED Master's Thesis September 1980
		6. PERFORMING ORG. REPORT NUMBER
7. AUTHOR(s) Ricky Eugene Shook		8. CONTRACT OR GRANT NUMBER(s)
9. PERFORMING ORGANIZATION NAME AND ADDRESS Naval Postgraduate School Monterey, California 93940		10. PROGRAM ELEMENT, PROJECT, TASK AREA & WORK UNIT NUMBERS
11. CONTROLLING OFFICE NAME AND ADDRESS Naval Postgraduate School Monterey, California 93940		12. REPORT DATE September 1980
		13. NUMBER OF PAGES 72
14. MONITORING AGENCY NAME & ADDRESS(If different from Controlling Office) Naval Postgraduate School Monterey, California 93940		15. SECURITY CLASS. (of this report) Unclassified
		15a. DECLASSIFICATION/DOWNGRADING SCHEDULE

16. DISTRIBUTION STATEMENT (of this Report)

Approved for public release; distribution unlimited.

17. DISTRIBUTION STATEMENT (of the abstract entered in Block 20, if different from Report)

18. SUPPLEMENTARY NOTES

19. KEY WORDS (Continue on reverse side if necessary and identify by block number)

Mathematical Models, Mixed Layers, Turbulent Boundary Layer, Mixing, Advection Ocean Thermal Structure; 1-Dimensional Numerical Model Turbulence

20. ABSTRACT (Continue on reverse side if necessary and identify by block number)

A one-dimensional mixed layer model (Garwood, 1976, 1977) is used to simulate the mixed layer depth and temperature observed during POLEX, a component of the North Pacific Experiment. POLEX occurred during January-February 1974 with mid-ocean observations (35°N, 155°W) of temperature and salinity made from R/P FLIP, while FLIP was under free-drift conditions. The results of this simulation show that apparent horizontal advection, due to the drift of R/P FLIP, was important in the heat and salinity budgets, but that vertical mixing and mixed layer depth changes were controlled primarily by the one-dimensional response of the turbulent kinetic energy budget to the local atmospheric forcing. Occasionally, surface salinity flux, due to large precipitation rates, can significantly alter (on the

DD FORM 1 JAN 73 1473   EDITION OF 1 NOV 65 IS OBSOLETE
(Page 1)   S/N 0102-014-6601

order of tens of meters) the thickness of ocean surface turbulent boundary layer, with demonstrated decrease in thickness during a single period of strong precipitation.

The One-Dimensionality of the Upper Ocean Mixing and the
Role of Advection During the POLE Experiment.

by

Ricky Eugene Shook
Lieutenant, United States Navy
B.S., Capital University, Columbus Ohio, 1973

Submitted in partial fulfillment of the
requirements for the degree of

MASTER OF SCIENCE IN OCEANOGRAPHY

from the
NAVAL POSTGRADUATE SCHOOL
September 1980

Author _____

Approved by: _____
                                                    Advisor

_____
                                                    Reader

_____
                          Chairman, Department of Oceanography

_____
                          Dean of Science and Engineering

3

ABSTRACT

A one-dimensional mixed layer model (Garwood, 1976, 1977) is used to simulate the mixed layer depth and temperature observed during POLEX, a component of the North Pacific Experiment. POLEX occurred during January-February 1974 with mid-ocean observations (35°N, 155°W) of temperature and salinity made from R/P FLIP, while FLIP was under free-drift conditions. The results of this simulation show that apparent horizontal advection, due to the drift of R/P FLIP, was important in the heat and salinity budgets, but that vertical mixing and mixed layer depth changes were controlled primarily by the one-dimensional response of the turbulent kinetic energy budget to the local atmospheric forcing. Occasionally, surface salinity flux, due to large precipitation rates, can significantly alter (on the order of tens of meters) the thickness of the ocean surface turbulent boundary layer, with a demonstrated decrease in thickness during a single period of strong precipitation.

4

TABLE OF CONTENTS

5

NOTATION

b	Buoyancy
$\overline{b'w'}$	Turbulent buoyancy flux ($cm^2 sec^{-3}$)
C	Degrees Centigrade
c_d	Non-dimensional drag coefficient
c_p	Heat capacity of sea water ($cal\ gm^{-1}C^{-1}$)
E	Rate of evaporation ($gm\ cm^{-2}sec^{-1}$)
E_a	Vapor pressure of air
E_s	Saturated vapor pressure of marine air
f	Coriolis parameter
g	Acceleration due to gravity
h	Turbulent boundary layer depth (modeled)
h_1	Mixed layer depth (modeled)
h_0	Observed mixed layer depth
m	Meters
P	Rate of precipitation ($gm\ cm^{-2}sec^{-1}$)
Q_a	Upward surface heat flux ($cal\ cm^{-2}sec^{-1}$)
Q_b	Back Radiation ($cal\ cm^{-2}sec^{-1}$)
Q_e	Latent heat flux ($cal\ cm^{-2}sec^{-1}$)
Q_h	Sensible heat flux ($cal\ cm^{-2}sec^{-1}$)
Q_0	Clear sky radiation ($cal\ cm^{-2}sec^{-1}$)
Q_T	Net surface heat flux ($cal\ cm^{-2}sec^{-1}$)
S	Salinity ($0/00$)
$\overline{S'w'}$	Turbulent salinity flux ($0/00\ cm\ sec^{-1}$)
T	Temperature

6

T_a	Temperature in the air
T_s	Sea-surface temperature
$\overline{T'w'}$	Turbulent temperature flux (mwatts cm^{-2})
t	Time (hours)
u_*	Frictional velocity at ocean surface
$\overline{U_a}$	Mean wind speed (m sec^{-1})
$\overline{u'w'}$	Vertical turbulent velocity flux
V	Velocity vector (cm sec^{-1})
V_c	Velocity vector due to ocean currents
V_e	Velocity vector due to Ekman flow
V_g	Velocity of current due to quasi-geostropic flow
V_p	Velocity due to the drift of R/P FLIP
w	Vertical component of turbulent velocity
z	Depth (meters)
dz	Depth increment
α	Expansion coefficient for heat
β	Expansion coefficient for salt
ρ	Density of sea water (gm cm^{-3})
ρ	Density of air (gm cm^{-3})
τ	Surface stress (dynes cm^{-2})
θ	Temperature
$\sim$	Represent the total instantaneous value
$< >$	Denotes the vertical average
Δ	Increment of change in a variable

ACKNOWLEDGEMENTS

The author wishes to express appreciation to Dr. R. W. Garwood, Department of Oceanography, Naval Postgraduate School, for his time, interest and guidance throughout this study, and to Dr. R. L. Elsberry for his helpful discussions and review of this thesis.

Finally, I would like to express my gratitude to my wife, Darlene, and to my son and daughter for their patience, understanding, and support during the last year.

I. INTRODUCTION

A. PURPOSE OF STUDY

The objective of this research was to investigate the conclusions which were reached by Simpson and Paulson [1979] from ocean data obtained as part of the Pole Experiment (POLEX), a component of the North Pacific Experiment (NORPAX). POLEX was part of the first process oriented NORPAX experiment. The experiment was named POLE to indicate that the horizontal extent of the sampling was small compared to the largest scales investigated in NORPAX. Simpson and Paulson concluded: "One-dimensional mixed-layer deepening models failed to predict the mixed-layer depth and temperatures observed during POLE. Horizontal advection, as evidenced from the salinity maximum frequently occurring at the bottom of the mixed layer and other *near-surface changes in salinity and temperature* not associated with local surface forcing, are responsible for the failure".[1]

This study will investigate the one-dimensionality of the POLE temperature and salinity data and determine if the mixed layer depth changes in response to the local atmospheric conditions (one-dimensional) or if these changes are caused by two and/or three dimensional advective processes. To accomplish this task, a non-stationary, one-dimensional bulk model of the mixed layer originally proposed by Garwood [1976, 1977]

---

[1] Simpson, J. J. and Paulson, C.A., 1979: Observation of Upper Ocean Temperature and Salinity Structure During POLE Experiment, J. Phys. Oceanogr., 9, page 869.

is expanded by including a salinity budget. A comparison of the results of a strictly one-dimensional model of the upper ocean with observations can be used to make an assessment of the one-dimensionality of the different variables which are involved in the upper ocean boundary layer response to the local atmospheric forcing.

One hypothesis to be examined is that horizontal advection may be important for the heat and salt budgets, and at the same time vertical mixing and mixed layer depth may be controlled primarily by one-dimensional or local forcing alone. One objective of this study will be to determine how responsive are the variables of heat and salt in the upper ocean boundary layer to one-dimensional effects. A second objective of this study is to use the data obtained as part of POLEX to see if the one-dimensional mixed layer model proposed by Garwood will predict the observed mixed layer depth, even if advection dominates the local changes in heat and salt content in the upper ocean.

The data used in this report contain observations made from R/P FLIP while under free-drift conditions. As a result of the free-drift condition of FLIP during the data collection period, advection as seen by R/P FLIP will be a combination of the actual advection in an Eulerian coordinate system for the area and advection due to the drift of FLIP. Henceforth, the term advection will be used to mean a combination of the actual advection term and apparent horizontal advection due to the drift of FLIP.

The data were collected during the period 28 January 74 through 14 February 74. During that time, FLIP occupied a station approximately 800 miles north of the Hawaiian Island Chain under free drift conditions. The position of FLIP ranged from 35°39'N, 155°05'W to

10

34°36'N, 155°25'W. The experimental site is hydrodynamically complex, as shown in Figure 1. The Subtropical Front is known to meander between 32° and 35°N (Roden, 1974; Barnett,1976). The region of the trade winds northeast of Hawaii has air-sea fluxes of latent heat in excess of 35 cal $cm^{-2}day^{-1}$ (Wyrtki, 1965). The Subtropical water mass formed in this region contrasts markedly with the less saline Eastern North Pacific Central Water characteristically encountered north of 35°N. The Horse Latitudes are located only 3° of latitude to the south of the observation area and the North Pacific Current is expected to affect the general hydrography of the region.

B. MILITARY IMPORTANCE

Mixed layer depth is an important factor when dealing with sound propagation in the ocean. It is used to determine such sonar detection variables as convergence zone distances, source level depth, and cutoff frequency for surface duct propagation. A model which could predict the change in mixed layer depth in response to the local atmospheric forcing could be incorporated in the existing acoustic models, for example the Fast Asymptotic Coherent Transmission (FACT) and the Naval Interim Surface Ship Model (NISSIM), presently being used at Fleet Numerical Oceanography Center (FNOC). A one dimensional mixed layer model would help the naval tactician to directly correlate the variability of the ocean with his weapon system and determine the most efficient deployment of the naval Anti-Submarine Warfare (ASW) assets.

C. LITERATURE REVIEW

The vertical fluxes of heat, salt, and momentum across the sea-air interface are the sources of almost all oceanic motions. In the fully

11

turbulent oceanic mixed layer bounded by the sea-air interface above and by the dynamically stable water mass below, the vertical fluxes are large. Below the mixed layer, they are usually negligibly small so that one can decouple the mixed layer from the underlying stable, quiescent water mass. This homogeneity is the root of the term "slab", which is often used to describe the layer as depicted in Figures 2 and 3.

When dealing with sound propagation in the ocean, the term mixed layer depth is sometimes taken to be that area with a uniform temperature structure, but this is not always the case. In Figure 4 the bottom of the mixed layer depth (Region I) appears to be at about 80 meters, and below there is a strong temperature gradient. However, examination of the σ_t profile shows that the mixed layer depth is about 30 meters. This shallow halocline was probably caused by an earlier rainfall which decreased the near-surface salinity. The assumption of vertical homogeneity in a bulk model, because of the problem associated with solving for the interior fluxes of buoyancy and momentum, reduces to the need to know only the surface and entrainment fluxes. However, only small vertical gradients in these mean variables may be associated with large turbulent fluxes. Therefore, the slab assumption should not be as automatically applied to the turbulent kinetic energy budget. The immediate local reaction of this mixed layer to those fluxes results in a homogeneous water column, i.e., vertical uniformity in the mean velocity and density. This adjustment to the density and velocity structure of the surface layers of the ocean to variable fluxes has been the subject of a large number of studies since Ekman's [1905] treatise where he originated the concept of a depth of frictional resistance for

the upper section of a wind stressed ocean. He further suggested that the wind-driven current will have a similar depth, the Ekman depth.

Much of the one-dimensional theory for the ocean surface turbulent boundary layer or mixed layer seems to be dependent upon the validity of two basic hypotheses. The first of these is that vertical mixing within the turbulent boundary layer and entrainment mixing at its base occur in response to local atmospheric forcing, i.e., the surface wind stress and net heat radiated or fluxed across the sea-air interface. The second hypothesis is that the mechanical energy budget is the key to the understanding and prediction of the mixed layer dynamics.

Most observations show that local atmospheric forcing such as an increase in wind speed increases the mixed layer depth and low wind speed and high solar radiation decreases mixed layer depth. This is less true with increased depth below the mixed layer. Observations by Pollard and Tarbel [1975] showed that horizontal coherence between the fluctuating wind-driven currents near the surface was large and consistent with the local amplitude and phase differences of the wind history. With increased depth, the horizontal coherence decreased monotonically as did the vertical coherence of the deeper current measurements with those near the surface. Kroll [1975] pointed out that the time scale of these strongly inertial currents is on the order of a couple of days, depending upon the stability of the underlying water column as well as the difference between the driving frequency and the local inertial frequency. The turbulent motions within the mixed layer are expected to be even more responsive to the local atmospheric conditions because of the small dissipation time scale for the turbulent kinetic energy--minutes

13

to hours, which depends upon the layer depth and turbulence intensity. Both the mean and turbulent kinetic energies in the mixed layer are expected to reflect the local boundary conditions for wind stress and surface buoyancy flux. Measurements of turbulent velocity fluctuations, which were made by Powell et al [1975] and Jones and Kenney [1977], show that the root-mean-square turbulent velocity does scale with the water surface friction velocity, u_*. Camp and Elsberry [1978] and Elsberry and Camp [1978] demonstrated the role of strong synoptic scale wind events for deepening. Garwood and Halpern [1976] and Elsberry and Raney [1978] indicated the importance of diurnal heating, especially at times between storms. Hindcasting simulations by Thompson [1976], Mellor and Durbin [1975] and Camp [1976] support the importance of surface boundary fluxes.

Kraus and Turner [1967] improved the one-dimensional model originally developed by Kraus and Rooth [1961]. This was accomplished by considering the turbulent kinetic energy budget utilizing the heat equation and a mechanical energy equation. Because the frictional generation of heat is negligible, the vertically integrated heat equation provides a relationship for the conservation of potential energy. They parameterized the mechanical production rate in terms of the friction velocity, but neglected the viscous rate of dissipation and the effects of entrainment shear production.

The application of mechanical energy principles to the problem of mixed layer dynamics has caused some disagreement. An important controversy in mixed layer modeling has been centered around whether mean kinetic energy or turbulent kinetic energy leads to the downward entrainment

14

buoyancy flux at the base of the turbulent boundary layer. The mean kinetic energy advocates, including Thompson [1976], Pollard [1977] and Price [1977], argue that this mean flow energy is directly converted to potential energy by a mean flow instability that causes the bulk Richardson number to be less than some critical constant of the order one. Turbulent kinetic energy advocates do not disagree with the possibility of this mechanism, but they argue it is not the dominant mechanism because turbulence-generated instabilities will usually sufficiently erode the interface to preclude the occurrence of the mean flow instability. De Szoeke and Rhines [1975] and Yun [1978] demonstrated that wind-shear production of turbulent energy is ultimately the most important source of energy for deepening the mixed layer, if the surface buoyancy flux is neglected. Even when the mean flow energy is important, they find that the rate of conversion of this energy to potential energy via entrainment shear production is controlled by the constraints of the turbulent kinetic energy budget. The Kraus-Turner turbulent energy model has not proven to be entirely satisfactory, and a number of changes have been suggested. Stevenson [1979] examined a number of alternative parameterizations for dissipation. Zeman and Tennekes [1975], Elsberry et al [1976], Alexander and Kim [1976] and Kim [1976] added depth-dependent dissipation terms that helped to reduce unrealistic deepening.

Garwood [1976, 1977] developed an ocean mixed-layer model using the Navier-Stokes equation of motion with the geostrophic component eliminated, the continuity equation in incompressible water, the heat equation from the first law of thermodynamics, the conservation of salt equation, and a linearized equation of state. The entrainment hypothesis depends upon

15

the relative distribution of turbulent energy between horizontal and vertical components and is offered as a plausible mechanism for governing both entrainment and layer retreat.

Garwood suggested that planetary rotation influences the dissipation of turbulence for deeper mixed layers and enables a cyclical steady state to exist on an annual basis. Furthermore, the rate of entrainment for the stable regime can not be a simple linear extrapolation of the unstable situaticns. Unlike the atomospheric boundary case, most of the solar radiation does not penetrate the layer. Therefore, downward turbulent heat flux in the oceanic boundary layer is as important as the upward flux during the course of both diurnal and annual cycles. The non-linearity of the interface entrainment tendency parameter, which is greatest for stable surface boundary conditions, results in a modulation of the long-term trend of the mixed-layer depth by the diurnal component of surface heat flux. In this model, buoyant production is somewhat more efficient than shear production as a source of energy for vertical mixing because of its unique effect on the vertical component of the turbulent velocity. The buoyancy equation is generated from the heat and salt equations together with an equation of state,

$$\bar{\rho} = \rho_0 \left[1 - \alpha \, (\tilde{\theta} - \theta_0) + \beta \, (\tilde{s} - S_0) \right] , \tag{1}$$

and the definition for buoyancy,

$$\tilde{b} = g \, (\rho_0 - \tilde{\rho})/\rho_0 \tag{2}$$

In equations 1 and 2 $\tilde{\theta}$ is temperature, $\tilde{S}$ salinity and ρ density while α and β are the expansion coefficients for heat and salt, respectively, and g is gravity. The tilde represents the total instantaneous

16

value and the subscript zero denotes a representative but arbitrary constant value. The generalization of using $\tilde{b}$ rather than $\tilde{\theta}$ will cast the model equations in a form equally applicable to those situations where evaporation and precipitation contribute significantly to the surface buoyancy flux and the structure of the evolving pycnocline. The buoyancy equation also has a more obvious and direct role in the mechanical energy budget as shown in Figure 5.

Miller [1976] included salinity in the mixed-layer model of Kraus and Turner [1967]. He concluded that salinity is important in determining the density structure when applying a mixed-layer model to the entire ocean, but the relative importance of salinity effect on the short term evolution of the density profile may not be significant. Paulus [1978] included salinity in the mixed layer model of Camp [1976]. He concluded that the effects of salinity structure were noticeable only in deepening regimes.

II. DATA ANALYSIS

A. METHODS

The upper ocean temperature and salinity data and the meterological data during the NORPAX POLE experiment were obtained from Simpson and Paulson [1977]. The parameters required for surface boundary condition computations, which are used in Garwood's model, include wind speed, wind direction, cloud cover, sea surface temperature, air temperature (dry bulb), dew point and rain code. These parameters were recorded at irregular time intervals. A linear interpolation technique was used to obtain values for these input parameters at regular time intervals. The resulting interpolated data were compared with the original data. Figures 6 through 12 show that no noticeable error was introduced into the parameters by the use of a linear interpolation.

Temperature and salinity profiles as in Figures 3 and 4 were digitized by using a Houston Instrument Hi Pad Digitizer and a Tektronix 4052 computer. The digitized profiles of temperature and salinity were linearly interpolated into hourly intervals. This provided for both initial conditions in the one-dimensional model and for fields to be used to compute observed mixed layer depth, $h_o(t)$, and to compare with subsequent model computations of $T(z,t)$ and $S(z,t)$.

B. SURFACE FLUXES

The mixed layer model uses the total surface heat flux ($Q_T(0)$), incident solar radiation, wind speed at a height d, rate of evaporation (E), and rate of precipitation (P) to calculate surface fluxes of

18

buoyancy (heat and salt) and momentum. The friction velocity, in air, is calculated using the following formulas:

$$\tau_s = \rho_a c_d \bar{u}_a^2 \qquad (3)$$

$$u_* = (\tau_s/\rho_a)^{1/2} \qquad (4)$$

where $\bar{u}_a$ is the mean wind speet (m/sec),

c_d is the non-dimensional drag coefficient (1.4×10^{-3}),

ρ_a is the density of air ($1.25 \times 10^{-3} gm/cm^3$), and

τ_s is the surface stress (dynes/cm^2).

The turbulent fluxes of latent heat (Q_e) and sensible heat (Q_h) are estimated using the following bulk aerodynamic formulas:

$$Q_e = c_d(.98E_s - E_a)\bar{u}_a \qquad (5)$$

$$Q_h = c_d(T_s - T_a)\bar{u}_a \qquad (6)$$

The net back radiation (Q_b) is estimated from the following empirical formula reported by Husby and Seckel [1975]:

$$Q_b = 1.14 \times 10^{-7}(273.16 + T_s)^4 (.39 - .05E_a^{1/2}) (1. - .6C^2) \qquad (7)$$

where E_s is the saturated vapor pressure of the marine air directly in contact with the sea surface (.98 corrects for salt defects),

T_a is the air temperature (degrees Centigrade),

E_a is the vapor pressure of air at approximately 10 m based on dew point temperature,

T_s is the sea-surface temperature (degrees Centigrade), and

C is the fractional cloud cover.

The upward heat flux is then:

$$Q_a = Q_e + Q_h + Q_b \qquad (8)$$

The solar insolation, Q_s, was estimated by:

$$Q_s = (1. - a\alpha^b)(1. - .66C^3)Q_0 \qquad (9)$$

The constants a and b are adapted from Tabata [1964] and the cubic cloud cover correction from Laevast [1960]. The coefficient C is the fractional cloud cover and α is the mid-day elevation angle of the sun. The clear sky radiation, Q_0, is given by

$$Q_0 = A_0 + A_1\cos\phi + B_1\sin\phi + A_2\cos2\phi + B_2\sin2\phi \qquad (10)$$

from the formula developed by Seckel and Beauday [1973]. The coefficients (A_0, etc.) were calculated by harmonic representation of the values presented in the Smithsonian Meteorological Tables (List, 1958) with

$\phi = (2\pi/365)(\dot{\tau}-21)$ where $\dot{\tau}$ is the julian day of the year. Turbulent temperature flux,

$$\overline{T'w'}(0) = -\frac{Qa}{\rho c_p} \qquad (11)$$

turbulent velocity flux,

$$\overline{u'w'}(0) = U_*^2 \qquad (12)$$

turbulent salinity flux,

$$\overline{S'w'}(0) = (P-E)S_{(0)} \qquad (13)$$

and turbulent buoyancy flux,

$$\overline{b'w'}(0) = g\left[\alpha\overline{T'w'}(0) - \beta\overline{S'w'}(0)\right] \qquad (14)$$

where α is the coefficient of thermal expansion,

    β is the coefficient of contraction of sea water due to salinity variations, and

    $S_{(0)}$ is the surface salinity value.

Figures 13, 14, 15 and 16 are graphs which show the hourly values of wind stress, τ, total heat flux at the surface, Q_T, salinity flux, $\overline{S'w'}$, and buoyancy flux, $\overline{b'w'}$, respectively, as calculated by the one-dimensional model. These figures can be compared with Figures 17 and 18 which show the interpolated hourly values of wind stress, τ, total heat flux at the surface, Q_T, buoyancy flux, $\overline{b'w'}$, and various other components which were reported by Simpson and Paulson [1977]. The values of these fluxes calculated here are nearly identical to the values reported by Simpson and Paulson. In Simpson and Paulson's graph on buoyancy flux (Figure 17), a positive buoyancy flux results when $Q_{net} > 0$. In the one-dimensional model (Figure 16) a positive buoyancy flux results when $Q_{net} < 0$ and $E > P$.

1. <u>Surface Wind Stress</u>

The wind stress calculated using the bulk approximation with a drag coefficient of 1.4×10^{-3} has a mean value of about 0.66 dynes cm^{-2} for the experimental period. Figure 13 shows the output for the surface wind stress as calculated by the one-dimensional model. Analysis of Figure 13 shows that for periods up to as long as 4 days the wind stress is considerably less than 1 dyne cm^{-2}, and it is evident that only two periods of relatively high winds were encountered during the experiment. One period of high wind near the middle of the experiment (time = 200-260 hours) with a maximum wind stress of 2.5 dynes cm^{-2}, and the other at the end of the experiment with a maximum wind stress of 3.3 dynes cm^{-2}.

2. <u>Surface Heat Flux</u>

Comparison of the total heat flux with net all-wave flux (Figures 17 and 19) shows that the net all-wave flux is generally the dominant term in the surface heat balance. However, a two-day period of enhanced

latent heat flux, due largely to a significant increase in wind speed

midway through the experiment (time = 250 hours), is evident when com-

paring Figures 13 and 14.

Simpson's [1977] calculation of the total heat budget for the

experiment suggested that the ocean gained 201 cal cm^{-2} for the time per-

iod from 3 Feb 74 - 12 Feb 74. Simpson's heat budgets calculations indi-

cated that ocean gained heat for 6 days, was in near thermal equilibrium

with the atmosphere for 2 days and lost heat to the atmosphere for 2-day

period. These results, coupled with the low wind stress, imply that the

upper dynamics might have been dominated by net surface heating for a

significant part of the experiment.

3. Salinity Flux

Figure 15 shows the salinity term as computed by the one-

dimensional model (equation 13) without including the precipitation term

in the computation. The precipitation term was omitted in the calculations

because no reasonable correlation could be made between a rain code given

in the experiment data report (Simpson and Paulson 1977) and an amount of

precipitation. The results of model runs which included precipitation

(estimated by the rain code) were compared to model runs which neglected

precipitation altogether. These model comparison runs showed no signifi-

cant difference except during one period when precipitation was much

larger than evaporation. Simpson and Paulson [1979] observed that over-

all evaporation and precipitation were in near equilibrium, with precip-

itation exceeding evaporation by 23 mg cm^{-2}.

4. Buoyancy Flux

Stratification in the ocean exerts a strong dynamical influence

on mixing since a stably stratified fluid requires work against buoyancy forces if mixing is to occur. For a stably stratified fluid, the density increases with depth and the buoyancy flux is directed downward, while the converse is true for an unstable, stratified fluid. In the one-dimensional model, surface buoyancy flux, $\overline{b'w'}_{(0)}$, is determined by the air-sea transfers (equation 14). Figure 16 shows the model computed buoyancy flux with $Q_{net} < 0$ and $E > P$ resulting in a positive buoyancy flux. The net heat flux, Figure 14, dominates the surface values of buoyancy flux during the experiment. During daytime periods, negative buoyancy flux results from the domination of the solar heating at the surface, while during the night periods a positive buoyancy flux is produced by the combined effect of net long-wave radiation and the up-ward turbulent fluxes of heat and moisture.

C. ADVECTION

The determination of the importance of advection to the heat and salt budget is necessary before an assessment can be made on how one-dimensional is the response of the variables of heat and salt are in the upper boundary layer. The velocity vector $\vec{V}$ of the advection term $(\vec{V} \cdot (\nabla T, \nabla S))$, is separated into two components in order to determine which component dominates the advection term.

1. Heat and Salinity Budgets

Neglecting internal sources and sinks, the equation for conservation of heat or salt is:

$$\int_{-d}^{0} \left[\underbrace{\frac{\partial(T,S)}{\partial t}}_{(a)} + \underbrace{\vec{V} \cdot \nabla(T,S)}_{(b)} + \underbrace{\frac{\partial \overline{(T,S)'w'}}{\partial z}}_{(c)} + \underbrace{\frac{\partial \overline{(T,S)'u'}}{\partial x}}_{(d)} + \underbrace{\frac{\partial \overline{(T,S)'v'}}{\partial y}}_{(e)} \right] dz = 0 \quad (15)$$

23

where T is heat, S is salinity, t is time, d is depth and $\vec{V}$ is the velocity vector in a coordinate system moving with the drifting platform. The meanings of these terms are:

(a) Heat or salinity change with time,

(b) Heat or salinity change due to advection in the moving coordinate system, assuming that when averaged over a day such features such as internal waves would not contribute to advection,

(c) Vertical heat or salt flux divergence, and

(d) and (e) Horizontal heat or salinity flux divergence.

Terms (d) and (e) are assumed to be small because they can not be evaluated. Therefore, equation (15) can be rewritten in terms of the variable temperature:

$$\int_{-d}^{0} \left[\frac{\partial T}{\partial t} + \vec{V}\cdot\nabla T \right] dz = - \underbrace{(\overline{T'w'}(0))}_{(f)} + \underbrace{\overline{T'w'}(d)}_{(g)} \qquad (16)$$

Term (f) is equal to the surface heat flux $Q_T/\rho c_p$, where Q_T is the net surface heat ($Q_T = Q_s - Q_b - Q_e - Q_h + Q_c$), cal cm^{-2} sec^{-1}, ρ is the density of sea water, 1 gm cm^{-3}, and c_p is the specific heat of sea water, 1 cal $gm^{-1}C^{-1}$. Term (g) is assumed to be negligible if d is well below the mixed layer, i.e., $d > h_{max}$. The vertical integrated mean advection of temperature is therefore,

$$-\int_{-d}^{0} (\overline{\vec{V}\cdot\nabla T})dz = \left[\frac{\left[\int_{-d}^{0}Tdz\right]_t - \left[\int_{-d}^{0}Tdz\right]_{t_0}}{\Delta t} \right] - \int_{t_0}^{t} \frac{Q_T dt}{\rho c_p} \qquad (17)$$

24

The same procedure used to derive (17) may be followed to find the average advective change in salinity. The surface salinity flux is given in equation (13). Thus the vertically integrated mean advection of salinity is:

$$\int_{-d}^{0} \overline{(\vec{V} \cdot \nabla S)} dz = \left[\frac{\left[\int_{-d}^{0} S dz \right]_t - \left[\int_{-d}^{0} S dz \right]_{t_0}}{\Delta t} \right] + \int_{t_0}^{t} S(E-P) dt \qquad (18)$$

The magnitude of actual advection (in an Eulerian coordinate system) can be checked by estimating $\vec{V}$ and ∇T or ∇S. The term $\overline{\vec{V} \cdot (\nabla T, \nabla S)}$, is the advection quantity averaged over a time interval, Δt. The velocity vector $\vec{V}$ can be separated into two components,

$$\vec{V} = \vec{V}_c + \vec{V}_p \qquad (19)$$

where $\vec{V}_c$ is the velocity vector due to the ocean currents and $\vec{V}_p$ is the velocity vector due to the drift of R/P FLIP. The velocity vector due to the ocean currents is itself composed of two components:

$$\vec{V}_c = \vec{V}_g + \vec{V}_e \qquad (20)$$

where $\vec{V}_g$ is the velocity of the current due to the quasi-geostrophic flow and is assumed to be parallel to the surface temperature contour. Therefore $\vec{V}_g \cdot \nabla T$ is assumed to be negligible. The order of magnitude of $\vec{V}_e$, the velocity current due to Ekman flow, is a function of the wind stress and can be estimated by,

$$|\vec{V}_e| = \frac{|\overline{\tau_w}|}{\rho h f} = 1.57 \text{ cm sec}^{-1} = 0.0565 \text{ km hour}^{-1} \qquad (21)$$

where $\overline{\tau_w}$ is the average wind stress, 0.66 dyn cm^{-2}, ρ is the density of sea water, h is average mixed layer depth, 5000 cm and f is the Coriolis

25

parameter, $2\omega\sin\phi$, where ω is the angular velocity of the earth and ϕ is the latitude.

The velocity calculated due to Ekman flow is insignificant when compared with the drift rate velocity calculated for R/P FLIP ($V_p=0.3$ km hour^{-1}) from 28 Jan 1974 to 14 Feb 1974. The calculated Ekman velocity is not sufficient enough to explain the drift of POLE. Hence, R/P FLIP was by no means flowing with the same mixed layer water mass throughout the experiment. Therefore, the velocity vector $\vec{V}$ will depend on the drift rate of R/P FLIP, $\vec{V} = \vec{V}_p$. What Simpson and Paulson [1979] call advection was not actual advection for the area but apparent advection due to the drift of R/P FLIP.

2. Calculation of the Rates of Advection

The distance R/P FLIP traveled from 0700 hours 28 Jan 1974 to 0700 hours 14 Feb 1974 (408 hours), was calculated to be 121 km, using a rhumbline distance calculation and a position of 35°36'N, 155°05'W to 34°36N, 155°25'W. Vertical profiles of temperature and salinity were taken from R/P FLIP from 0000 hours 30 Jan 1974 through 0700 hours Feb 1974 (total of 367 hours) which covered a distance of approximately 109 km. Figures 19 and 20 show the observed changes in heat and salt fluxes. The amounts of advection in a coordinate system moving horizontally with R/P FLIP were then estimated by subtracting the accumulated surface heat and salt fluxes from the changes in heat and salt content, respectively. Figures 21 and 22 show the results of this calculation. Least square fits were performed on the results, giving a slope of 2.0 cal cm^{-2}hour^{-1} for heat content gain and a slope of 0.45 ^{0}/00 cm hour^{-1} for salinity gain. These values can be used to

26

compute the average horizontal temperature and salinity gradients by multiplying by the total hours of observation (367 hours) and dividing by the average mixed layer depth (approximately 40m) and the distance FLIP traveled during the observational period (109 km),

$$|\nabla_H T| \approx 0.0017 \ C \ km^{-1} \tag{22}$$

$$|\nabla_H S| \approx 0.0004 \ ^0/00 \ km^{-1} \tag{23}$$

where $|\nabla_H T|$ is the horizontal temperature gradient and $|\nabla_H S|$ is the horizontal salinity gradient.

For comparison purposes, gradients were obtained from a NORPAC Atlas [1960] by dividing the atlas temperature change ($\Delta T = 0.2 \ ^\circ C$) and the atlas salinity change ($\Delta S = 0.05 \ ^0/00$) between FLIP starting and final positions (35°39'N, 155°05'W to 34°36'N, 155°25'W) by the total distance (121 km) which FLIP traveled,

$$|\nabla_H T|_A = 0.0017^\circ C \ km^{-1}$$

$$|\nabla_H T|_A = 0.0004 \ ^0/00 \ km^{-1}$$

where $|\nabla_H T|_A$ and $|\nabla_H S|_A$ are the horizontal temperature and salinity gradients that were calculated from the NORPAC Atlas. Although these values agree with the earlier calculation, equations (22) and (23), they were only obtained to show agreement in order of magnitude with recorded atlas values. These results further illustrate the fact that what Simpson and Paulson [1979] call advection was probably the result of the drift of R/P FLIP.

Figures 19 and 21 show that the temperature field, which is a function of both time and depth, has large fluctuations which can only be explained by advection, or the drift of FLIP which is a non one-dimensional effect. These large fluctuations dominate the heat budget

27

on the time scales shorter than 100 hours, but over a longer time scale, surface flux is equally important (one-dimensional effects). Figure 23 is a plot of observed sea surface temperature and a plot of the model-computed mixed layer temperature, with the model-computed temperature slightly offset on the temperature scale for comparison. Comparing the two plots, a one-dimensional component can be detected in the observed sea surface temperature time series but the stronger component due to the drift of FLIP is evident. Therefore, this apparent advection (as seen by FLIP) of temperature is important on all time scales, but dominates the short time scale. Figures 20 and 22 show that advection of salinity dominates the salinity budget over both the short and long time scales up to at least 400 hours, which was the period of observations.

D. MIXED LAYER DEPTH

1. Observed Mixed Layer Depth

The observed mixed layer depth, shown in Figure 17 as used by Simpson and Paulson [1979], is the shallowest depth at which the density is not more than 0.02 σ_t units greater than the density at a depth of 5 m. However, salinity and temperature changes can occur above z = 5m. In such cases, the above definition will result in a misleading computed time series for mixed layer depth. A more practical definition for observed mixed layer depth, which would be more consistent with the precision of the available POLEX observational data, would be the shallowest depth at which the observed value of σ_t is 0.02 σ_t units greater than the observed surface value. For comparison with the Garwood model, the observed mixed layer depth (h_0) will be defined according to this latter definition.

28

Contours of temperature for the observation period are shown in Figures 24 and 25. Figure 24, which is based on a contour interval of 0.5 C, shows a mixed layer depth as varying from near the surface to approximately 90 meters. Figure 25, which has a contour interval of 0.05 C after having been smoothed twice,[2] shows a mixed layer from near the surface to approximately 80 meters. This illustrates the importance of resolution when determining mixed layer depth from temperature contours. A higher resolution frequently results in a shallower mixed layer depth. Therefore, a temperature contour interval of 0.5 C is not sufficient resolution to accurately determine mixed layer depth from the contour plot. Although density is a function of both temperature and salinity, during this time series the salinity influence was not significant, so that the density was mainly dependent upon temperature. A mixed layer depth definition could then be defined as the shallowest depth at which the temperature is not more than 0.1 C less than the temperature at the surface which would compare well with the similar definition based on the observed density structure, as is evident by comparing Figure 25 with the observed mixed layer depth in Figure 26.

2. Comparison of the Model-Computed Mixed Layer Depth with Observed Mixed Layer Depth

Figure 26 is a time series of the depth of the model computed turbulent boundary layer, $-h(t)$, and of the observed mixed layer depth, $-h_0(t)$. The value of h should be less than or equal to the mixed layer depth as determined from observed $\partial \rho / \partial z$ if the model simulation of the

_____

[2] Smoothing was accomplished by giving the center data point a weight of 2 and all of the surrounding data points a weight of 1.

29

vertical density structure changes are accurate. Figure 27 is a plot of the same functions, $h(t)$ and $h_0(t)$ between time = 200 hours and time = 400 hours. Notice that the model results compare favorably with the observations except for a period of about one day starting at hour 285. Figure 28 is the model computed mixed layer depth, $h_1(t)$. The value of $-h_1(t)$ is taken to be the depth at which the model σ_t is $0.02\sigma_t$ units greater than the value of $<\sigma_t>$ where $< >$ denotes the vertical average for the turbulent boundary layer. This definition is equivalent to that for $h_0(t)$ if the turbulent boundary layer is homogeneous. Figure 29 shows both $h_1(t)$ and the observed mixed layer depth, $h_0(t)$ for the same time period as Figure 28. Notice that $h_1 \leq h$ for all t. Although $h_0(t)$ compares well with $h(t)$, there are times during which $h_0(t)$ is more comparable to $h_1(t)$. For example, for the period between t = 285 hours and t = 310 hours, $h_0(t)$ is most similar to $h_1(t)$. This happens because, although the turbulent boundary layer may be quite shallow, the associated transient thermocline is not sufficiently strong to influence the values for $h_1(t)$ and $h_0(t)$.

Only during one time period, at about time = 100, is the observed mixed layer depth found to be significantly deeper than either the turbulent boundary layer, $h(t)$, or the mixed layer depth, $h_1(t)$, computed by the model. This difference between the predicted and observed mixed layer depth could be the result of R/P FLIP drifting through a warm core eddy or filament of water mass having more tropical characteristics. Figures 21 and 22, which are the graphs of the advective components of the heat and salt budgets, show a large increase in the magnitudes of both the advection of heat and salt at about time = 100 hours. This

large increase in advection of both heat and salt is consistent with the
hypothesis that R/P FLIP drifted across either an eddy or a filament of
water from the south of the Subtropical front. The Subtropical water
mass which lies to the south is warmer and more saline than the Eastern
North Pacific Central water.

3. Salinity Effects on the Mixed Layer Depth

An additional model simulation was conducted in order to deter-
mine what effect precipitation has on the mixed layer depth. A steady
rate of precipitation of 5×10^{-5} gm cm^{-2}sec^{-1} was prescribed over a 12-
hour period starting at t = 200 hours. At all other times precipitation
was assumed to be negligible. This event corresponds in magnitude, at
least, with the rate of precipitation reported by Simpson [1977] for
5 February 1974. Figure 30 shows a rapid decrease in the surface salin-
ity with the injection of the precipitation. It drops from about 34.11 ^{0}/oo
to 33.99 ^{0}/oo. This drop in surface salinity causes a rapid rise in the
surface salinity flux as shown in Figure 31. Figure 32 shows the model
prediction of the mixed layer depth with and without the precipitation
event. The associated increase in downward buoyancy flux, $\overline{b'w'}_{(0)}$, due
to the increase in salinity flux (Figure 31) caused the model mixed
layer depth to deepen much less rapidly than for the case without pre-
cipitation. The effect would have been even more apparent if the pre-
cipitation period had not coincided with strong winds.

Analysis of Figure 29 shows that the turbulent boundary layer
depth predicted by the model was approximately 20 meters deeper than the
observed mixed layer depth at t $\approx$ 210 hours. This time period coincides
with that reported by Simpson and Paulson [1979] as the period of most

31

intense precipitation. These results suggest that, if the amount of
precipitation were accurately known and included in the model boundary
conditions, there would be an even better correlation between the model
mixed layer depth and the observed mixed layer depth.

III. SUMMARY

This analysis of 15 days of salinity, temperature and density pro-
files from R/P FLIP as part of the NORPAX POLE experiment and the ac-
companying model study suggest that, non one-dimensional effects were
very important for both the heat and salt budgets. Vertical mixing and
mixed layer depth are controlled primarily by the one-dimensional response
of the turbulent kinetic energy budget to the local atmospheric forcing.
It is apparent that the non one-dimensional effects may be largely ex-
plained by the drift of R/P FLIP. Results from POLE site showed that this
apparent horizontal temperature advection (as observed by the moving plat-
form) was important on all time scales and dominated the small time scale.
Nevertheless, the one-dimensional model computation of mixed layer depth
compared favorably with the observed mixed layer depth. It is interest-
ing that even though this apparent advection usually dominated the salt
budget over both the long and short time scales, the one-dimensional mixed
layer model response to the surface salinity flux can be significant.
During the single period of strong precipitation, the mixed layer depth
was shallower (on the order of tens of meters) than it would have been
without precipitation. This is consistent with the results of Miller
[1976], showing that salinity flux can at least occasionally play an
important part in mixed layer dynamics in the subtropics. Further
studies would have to be conducted with observational data that included
the time, duration, and amount of precipitation before a firm conclusion
can be made on the longer-term importance of salinity effects on the

33

mixed layer depth. Qualitatively, model performance was improved when the influence of precipitation was taken into account.

Simpson and Paulson [1979] concluded that the one-dimensional models failed to predict the mixed layer depth and temperature observed during POLE. Why did the models of Pollard et al [1973] and Niiler [1975], which were used by Simpson and Paulson, fail to predict the observed mixed layer depth?_ One part of the explanation for the model's apparent failure could be the definition of mixed layer depth used by Simpson and Paulson. An accurate determination of the mixed layer depth from a vertical profile can only be made by considering the entire profile, an erroneous analysis of the mixed layer depth is probable whenever there is a transient pycnocline above z = 5 meters. Therefore, contrary to the results of Simpson and Paulson [1979], it has been shown that the one-dimensional turbulence closure model used here does seem to explain most of the observed mixed layer depth changes and that the mixed layer depth is more influenced by the local surface fluxes than by horizontal advection.
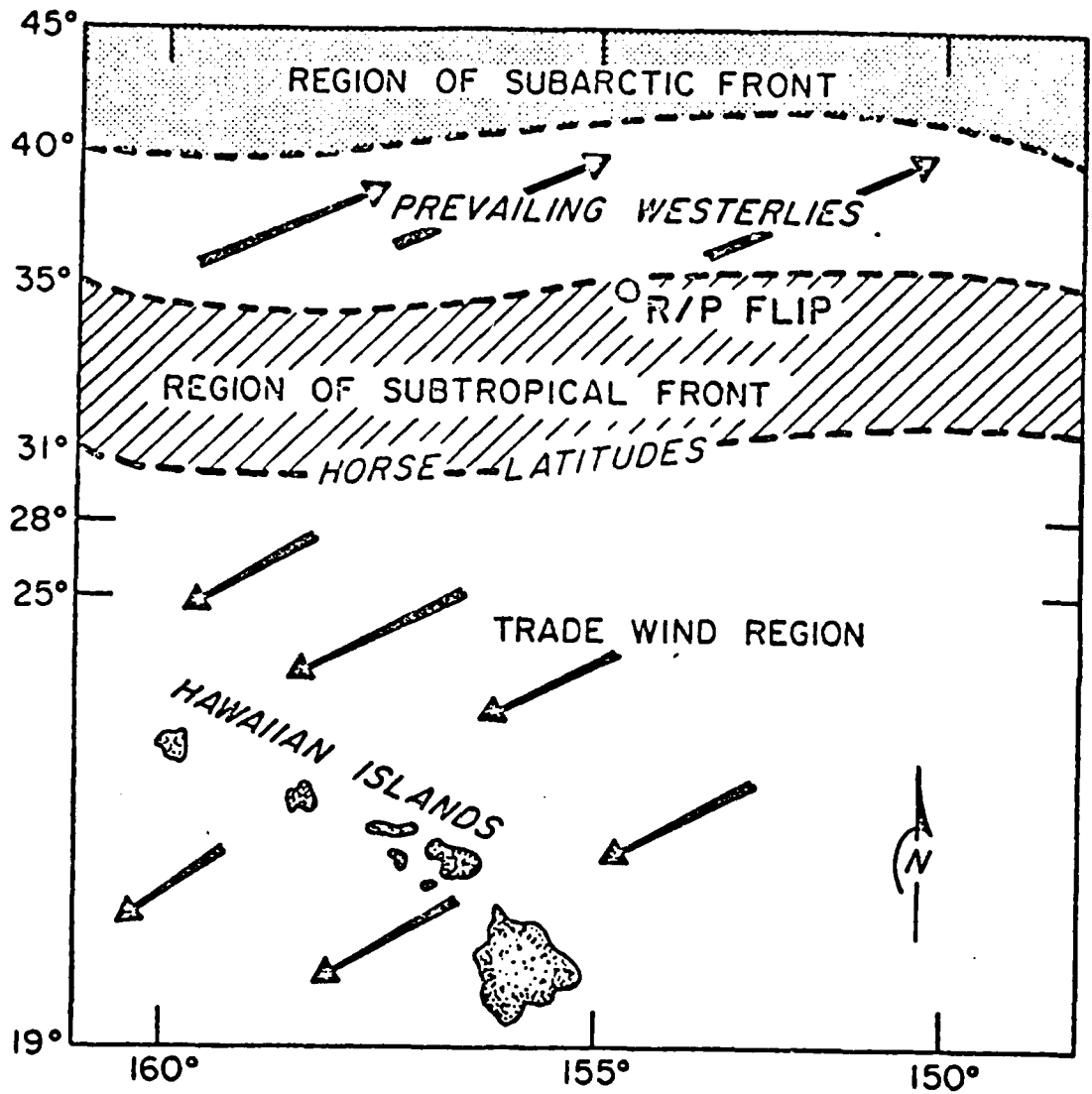
Figure 1. The location of the R/P FLIP during the POLE
experiment (35°N, 155°W) in relation to general
oceanic features. (Simpson and Paulson 1977)
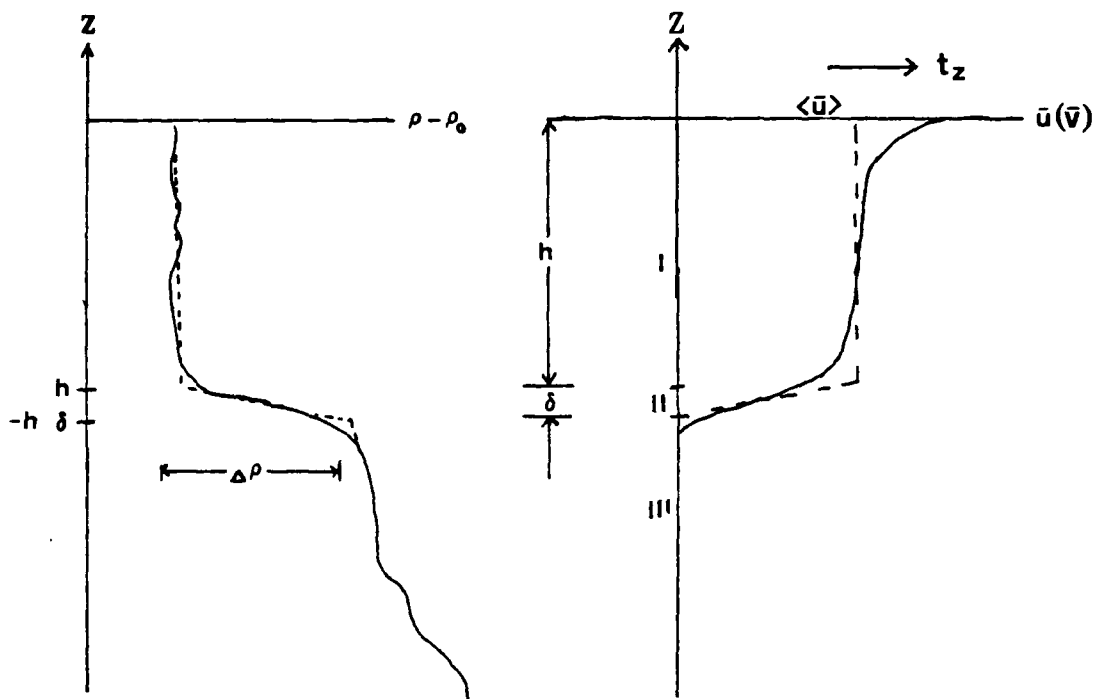
Figure 2. Idealized density and mean velocity profiles of the ocean
mixed layer (----). Mixed layer depth is (h), (δ) is the
thickness of the interface or entrainment zone. Region I
is the fully turbulent mixed layer depth. Region II is the
slightly stable, intermittently-turbulent entrainment zone.
Region III is the stable underlying watermass having negli-
gible vertical fluxes in comparison to those of Region I.
(Garwood 1977)

36
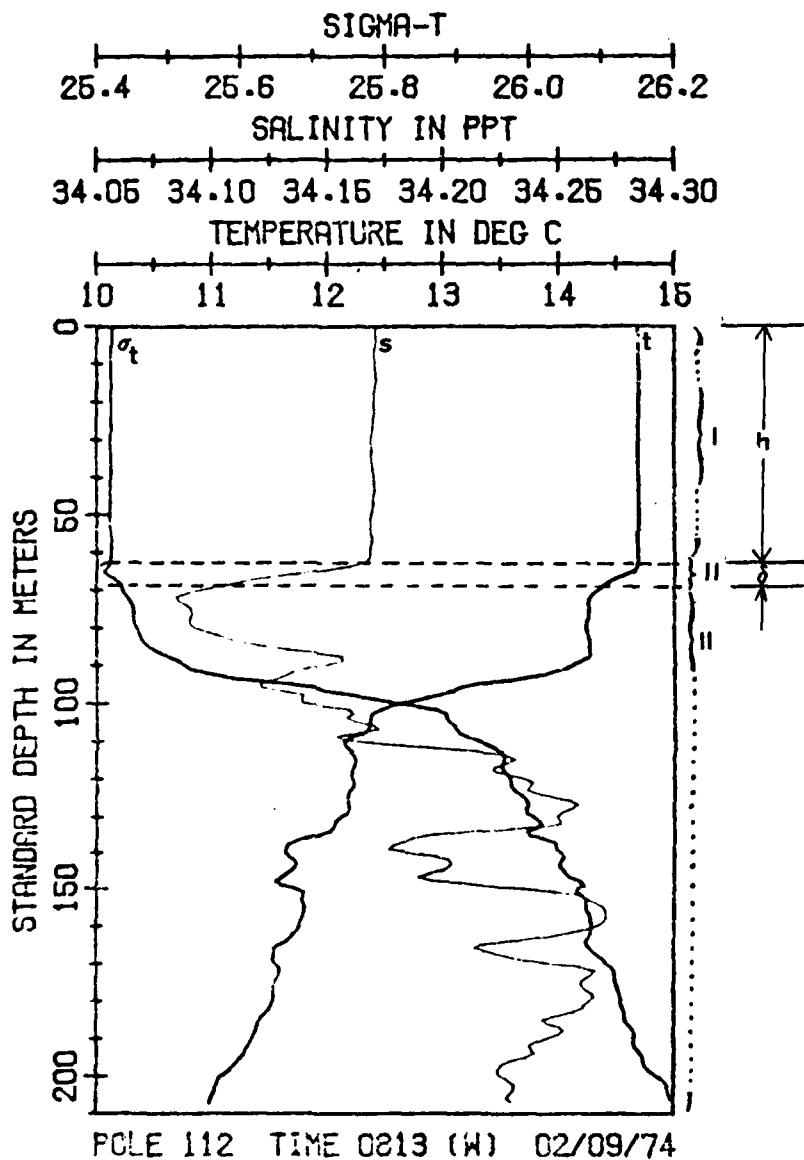
Figure 3. Typical POLEX data temperature, salinity, and sigma-t pro-
files taken from Simpson and Paulson [1979]. Added to the
profile is Region I the fully-turbulent mixed layer of
depth h. Region II the slightly stable, intermittently-
turbulent entrainment zone of thickness δ. Region III is
the stable underlying water mass having negligible fluxes
in comparison to those of Region I.

37

SIGMA-T

25.4	25.6	25.8	26.0	26.2	26.4

SALINITY IN PPT

34.05	34.10	34.15	34.20	34.25

TEMPERATURE IN DEG C

10	11	12	13	14	15

POLE 046   TIME 0604 (W)   02/03/74
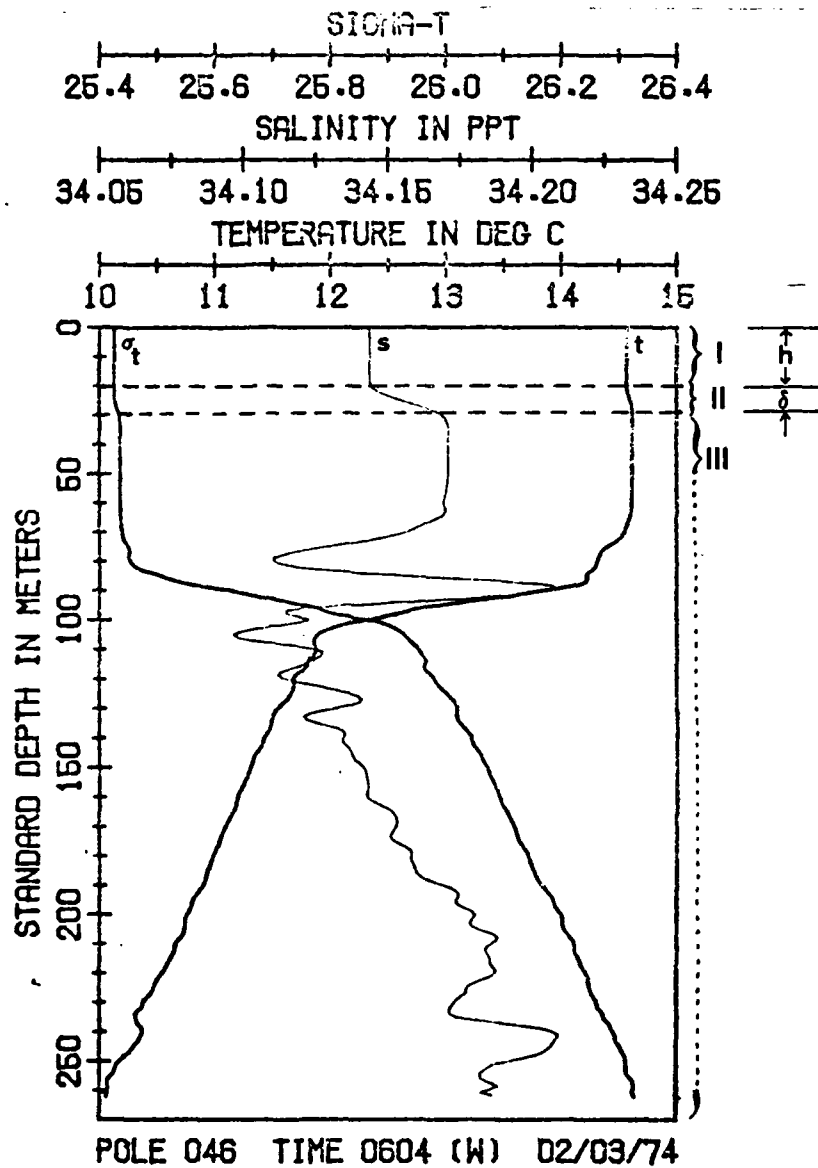
Figure 4.   Typical POLEX data temperature, salinity, and sigma-t profiles taken from Simpson and Paulson [1979]. Added to the profile is Region I the fully-turbulent mixed layer of depth h. Region II the slightly stable, intermittently-turbulent entrainment zone of thickness δ. Region III is the stable underlying water mass having negligible fluxes in comparison to those of Region I.

38

$U_* b_*$

NET SURFACE BUOYANCY FLUX
PLUS ABSORPTION OF SOLAR RADIATION

ENTRAINMENT BUOYANCY FLUX *

P.E. = P.E. (t_0)

$-\rho_0 \int_{t_0}^{t} \int_{-h-\delta}^{0} \overline{bw}\, dz\, dt$

INTERIOR BUOYANCY FLUX

VERTICAL TURB. K.E.

$\frac{1}{2}\rho_0 \int_{-h-\delta}^{0} \overline{w^2}\, dZ$

REDISTRIBUTION *

DISSIPATION *

HEAT

$\tau \cdot u(o)$
WORK BY WIND STRESS

MEAN K.E.

$\frac{1}{2}\rho_0 \int_{-h-\delta} (U^2 + V^2)\, dZ$

SHEAR PRODUCTION *

HORIZONTAL TURB. K.E.

$\frac{1}{2}\rho_0 \int_{-h-\delta}^{0} \overline{u^2 + v^2}\, dZ$
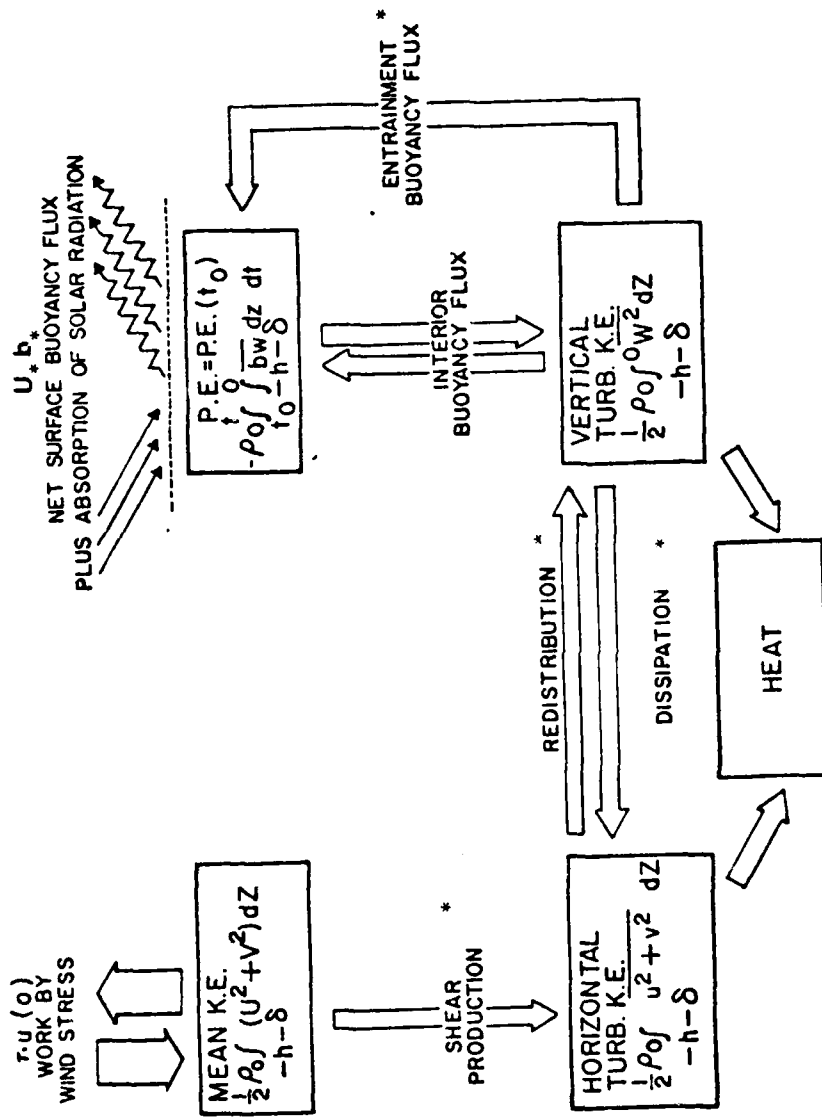
Figure 5. Mechanical energy budget for the ocean mixed layer. Asterisks indicate those processes that must be parameterized to close the system of equations. (Garwood 1977)

39

TIME (Julian Date)

METERS SEC⁻¹
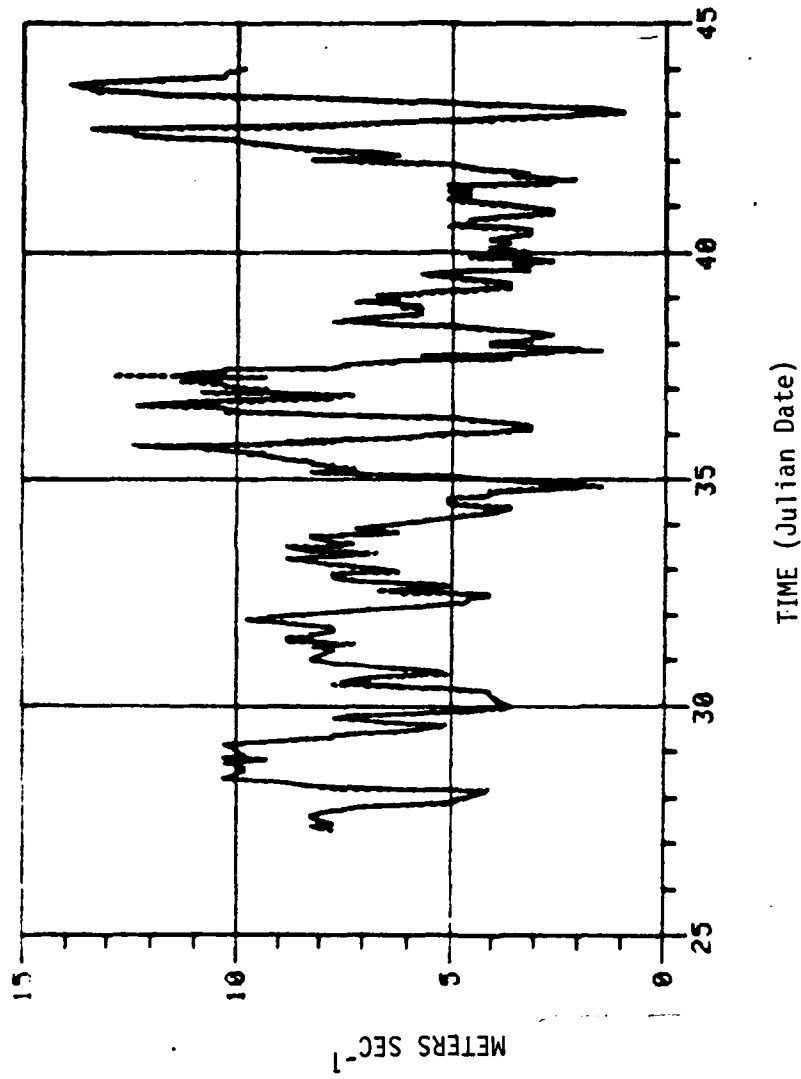
Figure 6.   Interpolated wind speeds (dashed line) and
            measured wind speeds (solid line)

40
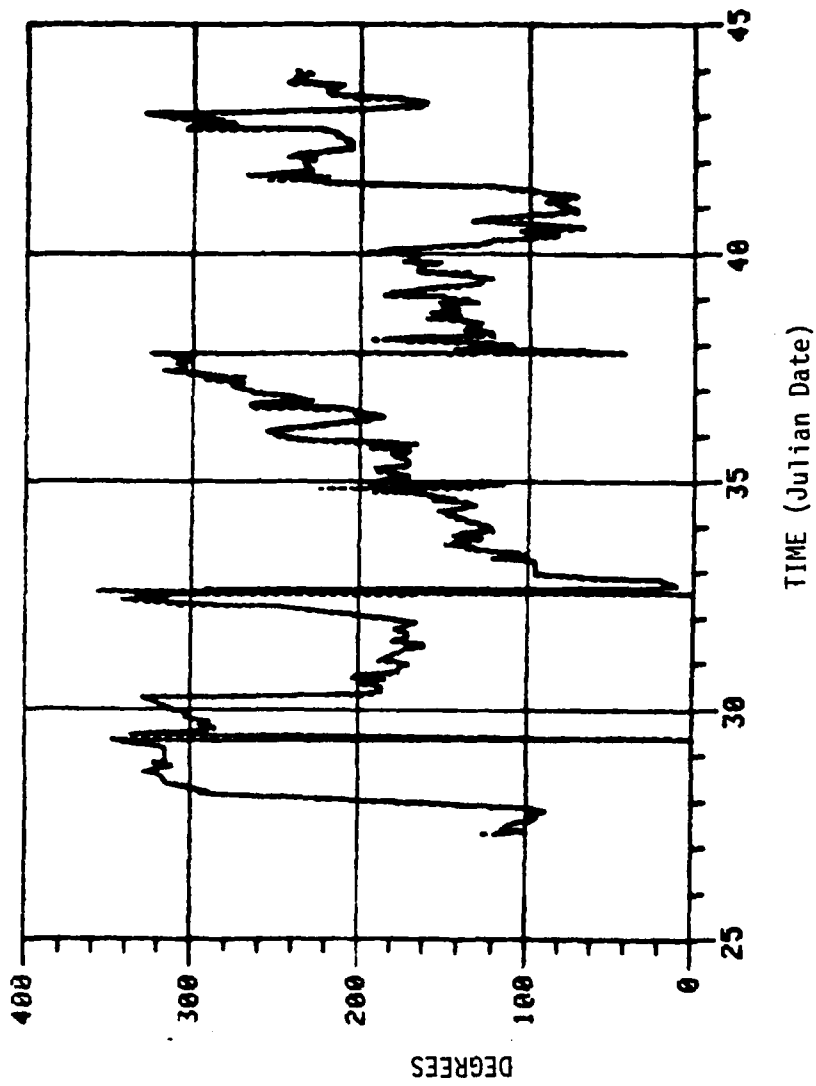
Figure 7.   Interpolated wind direction (dahsed line) and
measured wind direction (solid line).

41
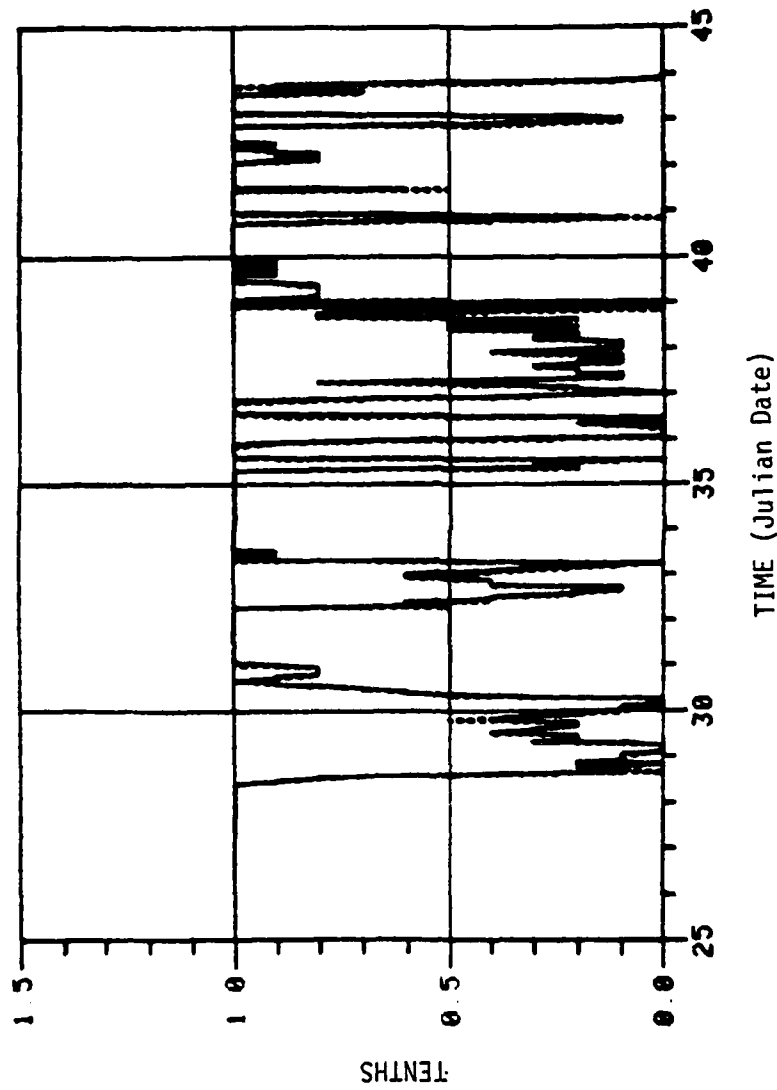
Figure 8. Interpolated cloud cover, scale of 0 to 1.0 (dashed line) and measured cloud cover (solid line).

42.
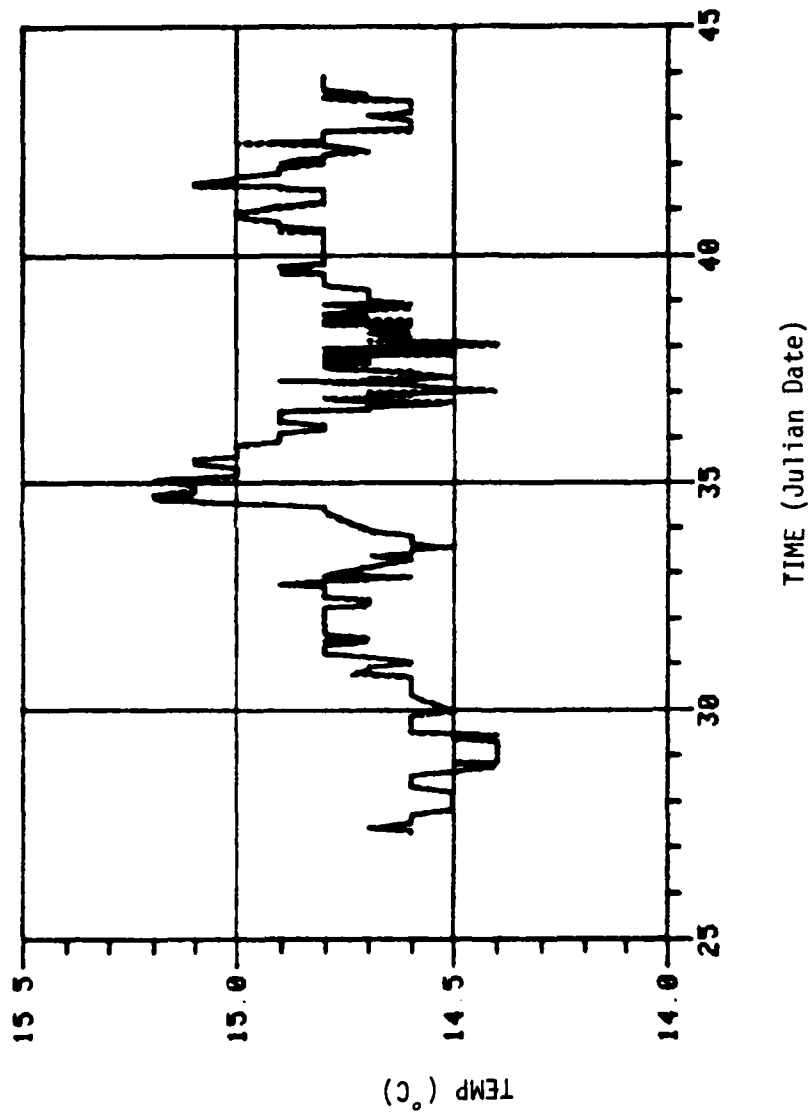
Figure 9.   Interpolated sea surface temperature (dashed line)
and measured sea surface temperature (solid line).

43
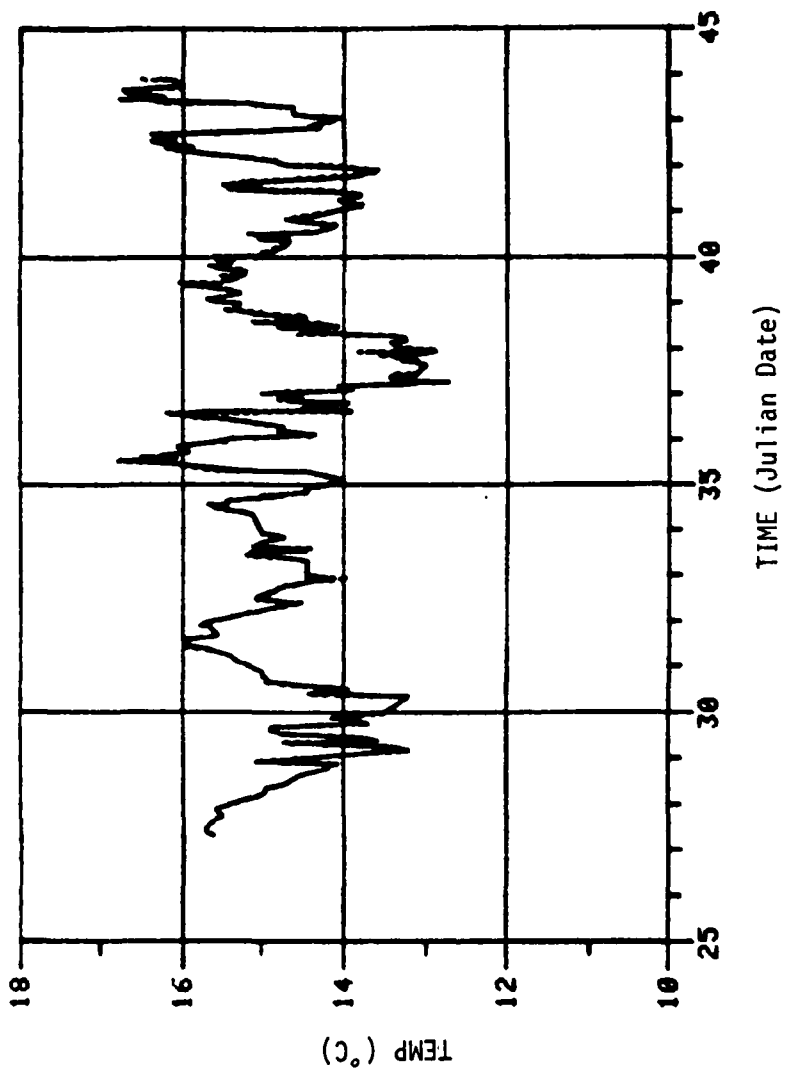
Figure 10. Interpolated air temperature, dry bulb (dashed line)
and measured air temperature, dry bulb (solid line).

44
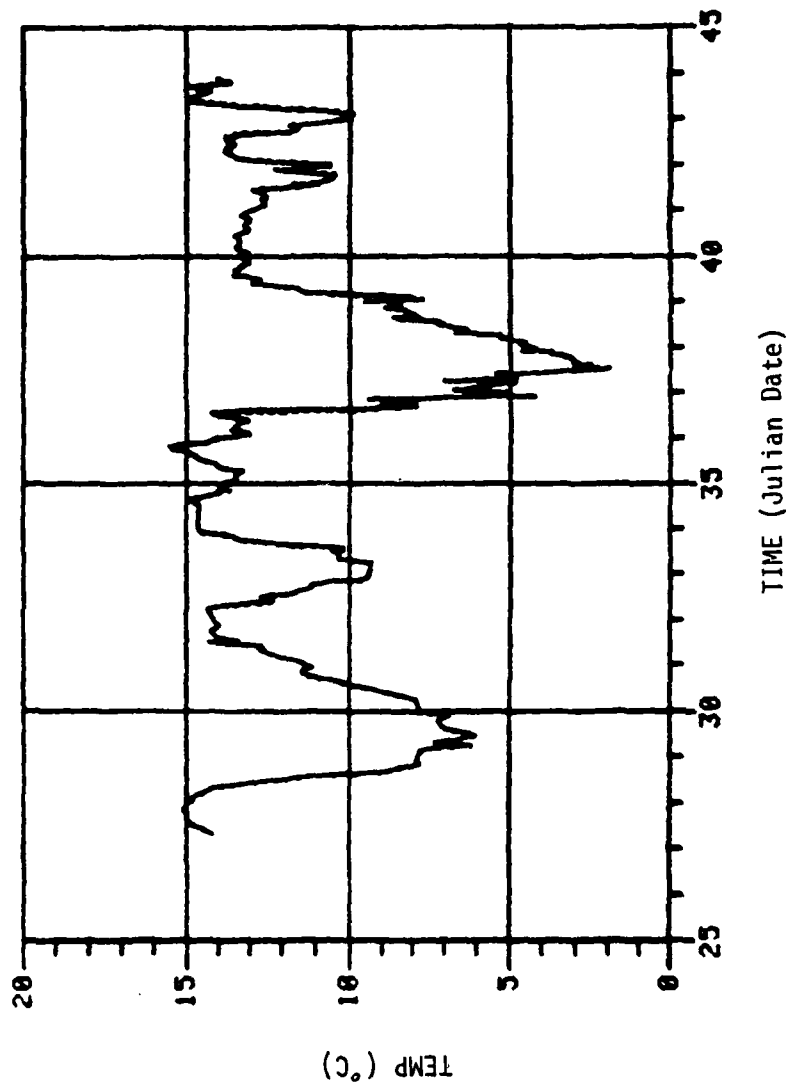
Figure 11. Interpolated dew point (dashed line) and
measured dew point (solid line).

45
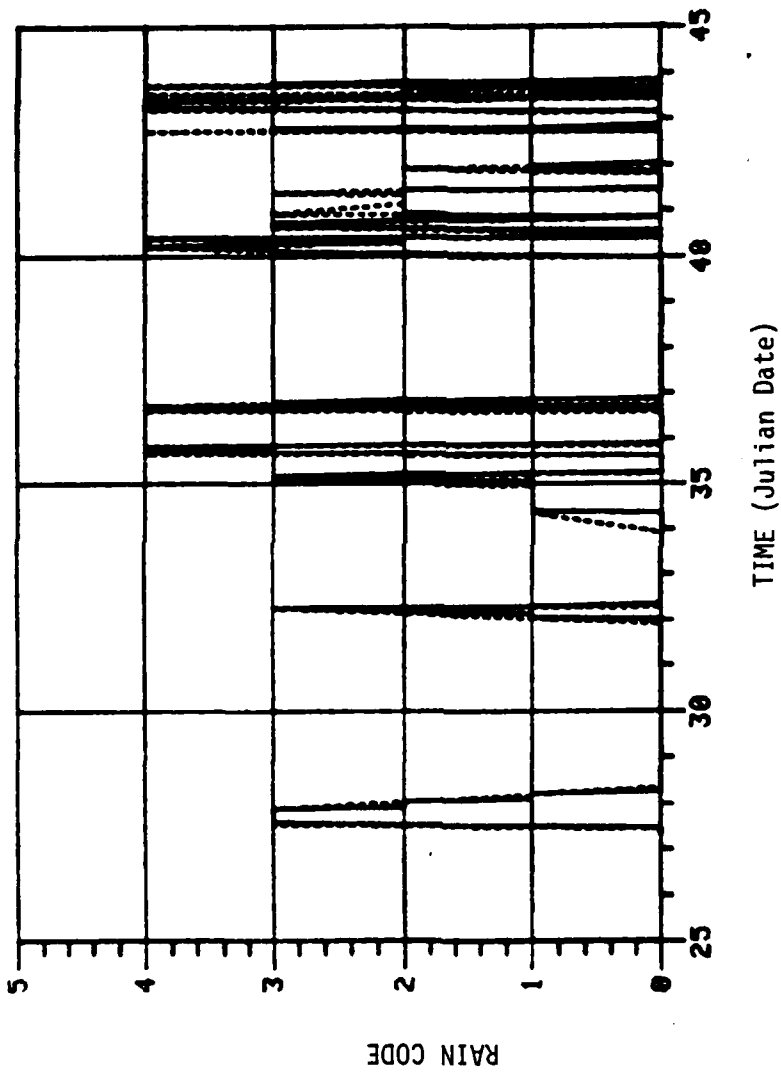
Figure 12. Interpolated rain code (dashed line) and
measured rain code (solid line).
Rain Code: 0-no rain, 1-fog, 2-mist, 3-light rain,
4-rain.

46
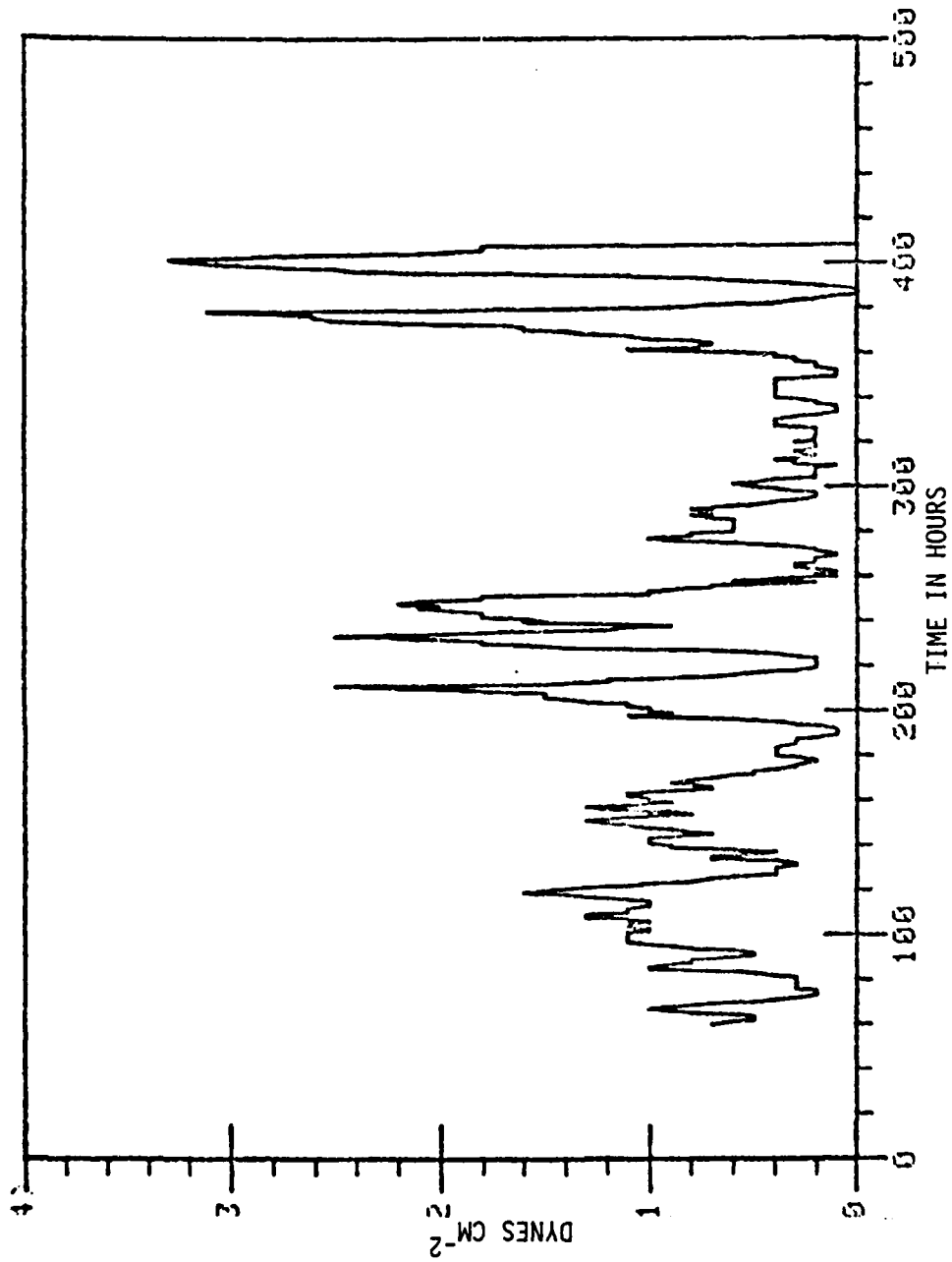
Figure 13. Model-computed hourly values of the wind stress (τ).
The origin of the abscissa is 1000 GMT 28 January 1974.

47
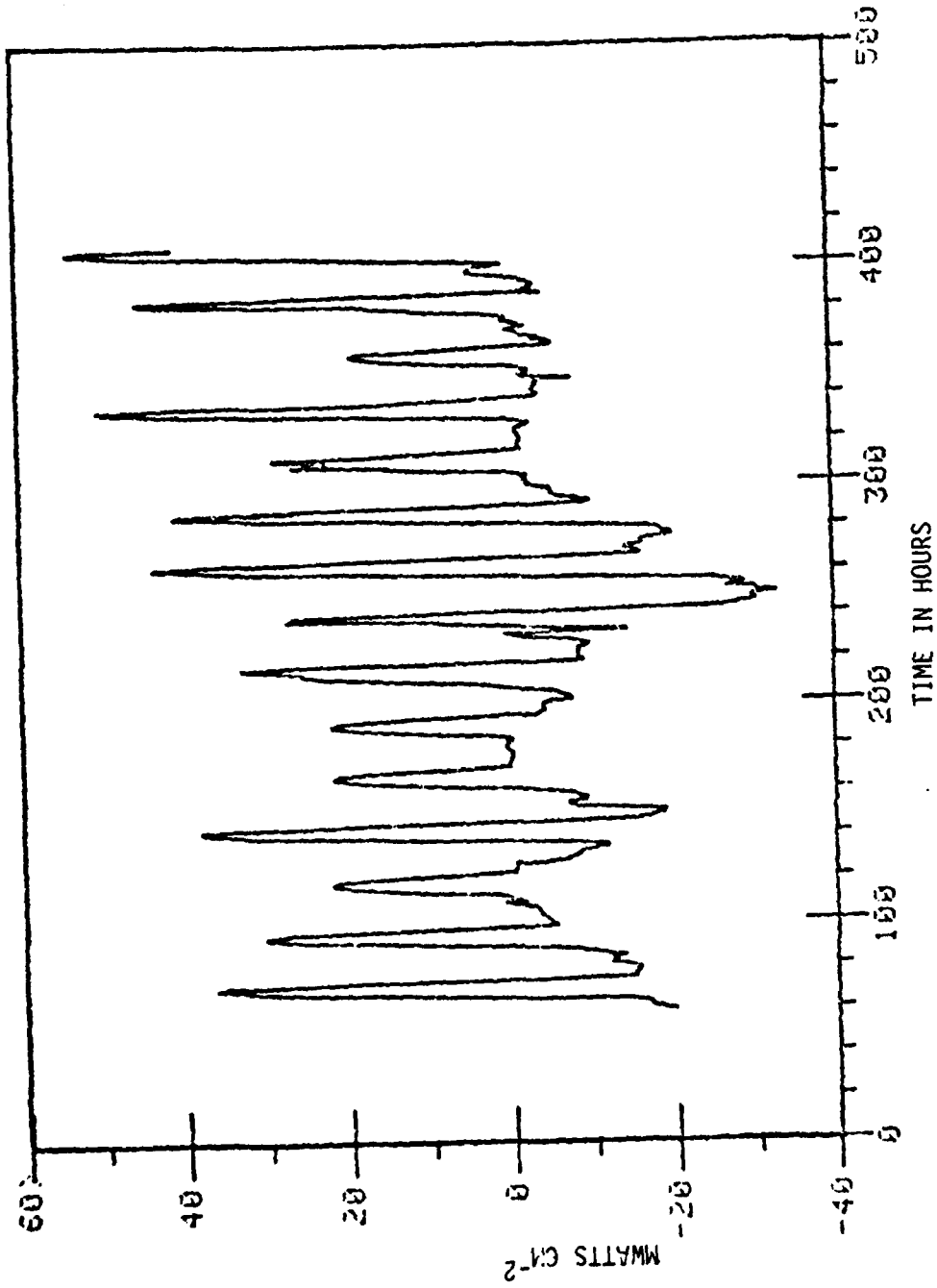
Figure 14. Model computed hourly values of the total downward heat flux at the surface. The origin of the abcissa is 1000 GMT 28 January 1974.
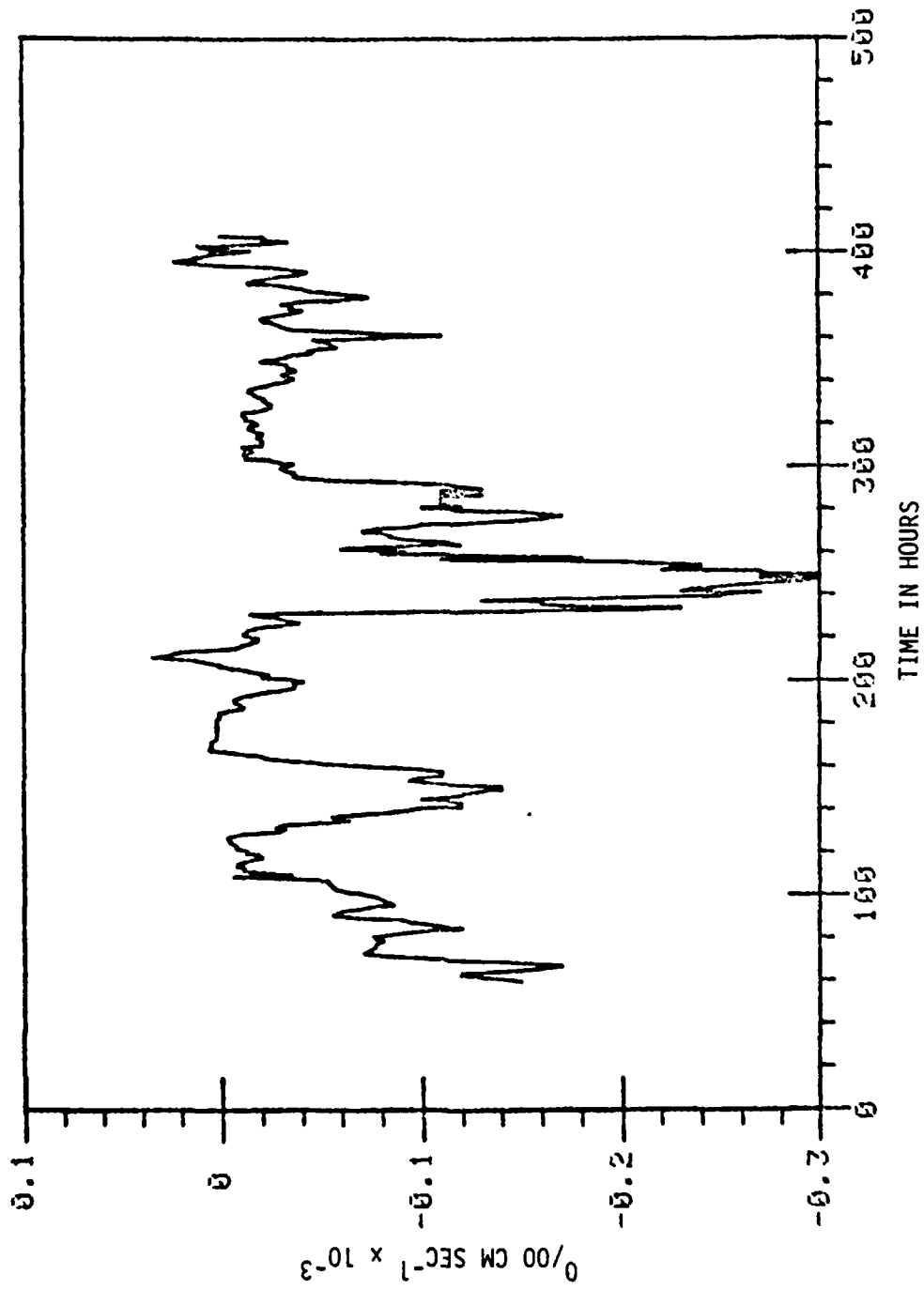
Figure 15. Model computed hourly values of salinity flux ($\overline{S'w'}$), neglecting precipitation.

49
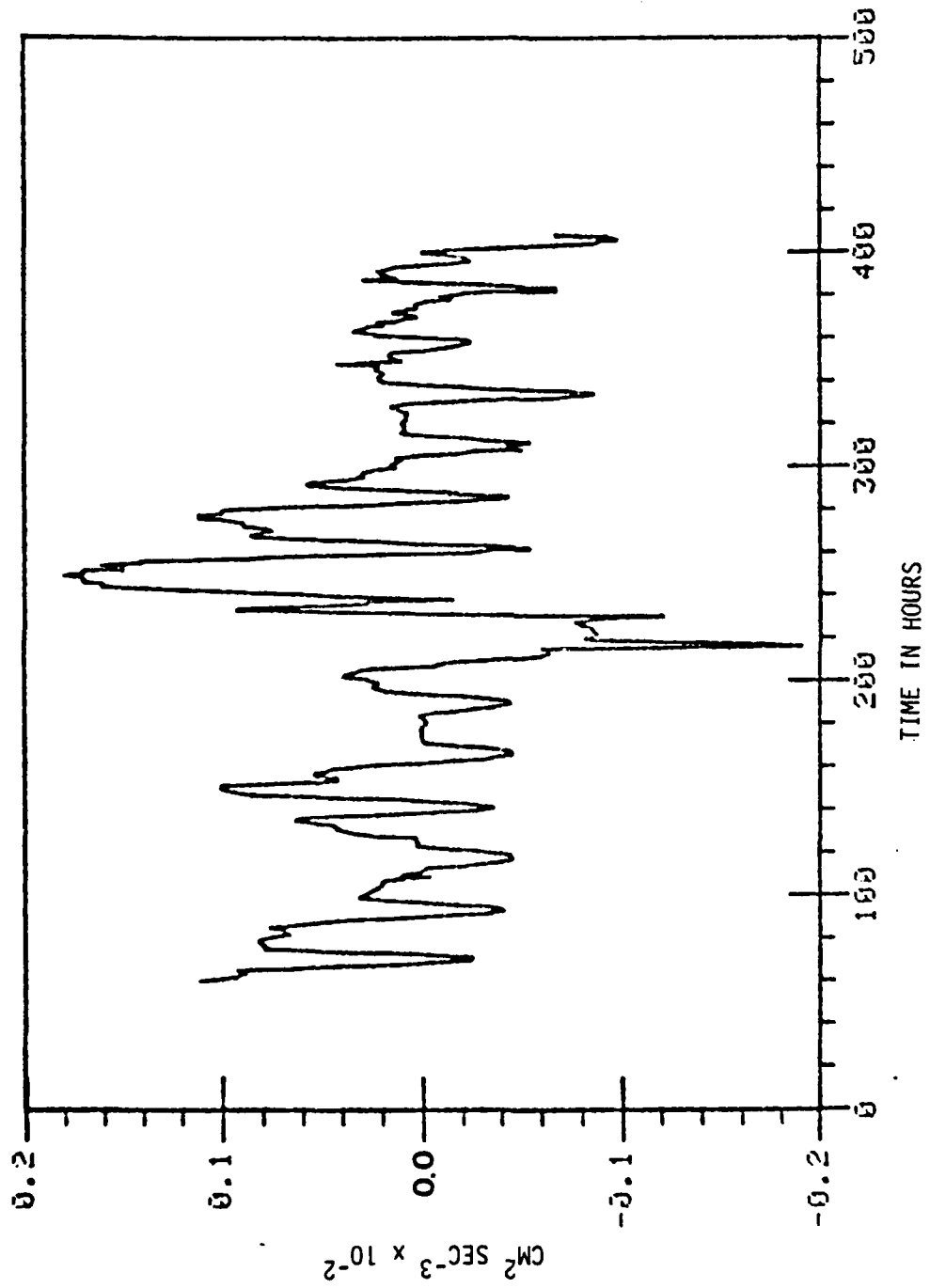
Figure 16. Model computed hourly values of buoyancy flux ($\overline{b'w'}$).
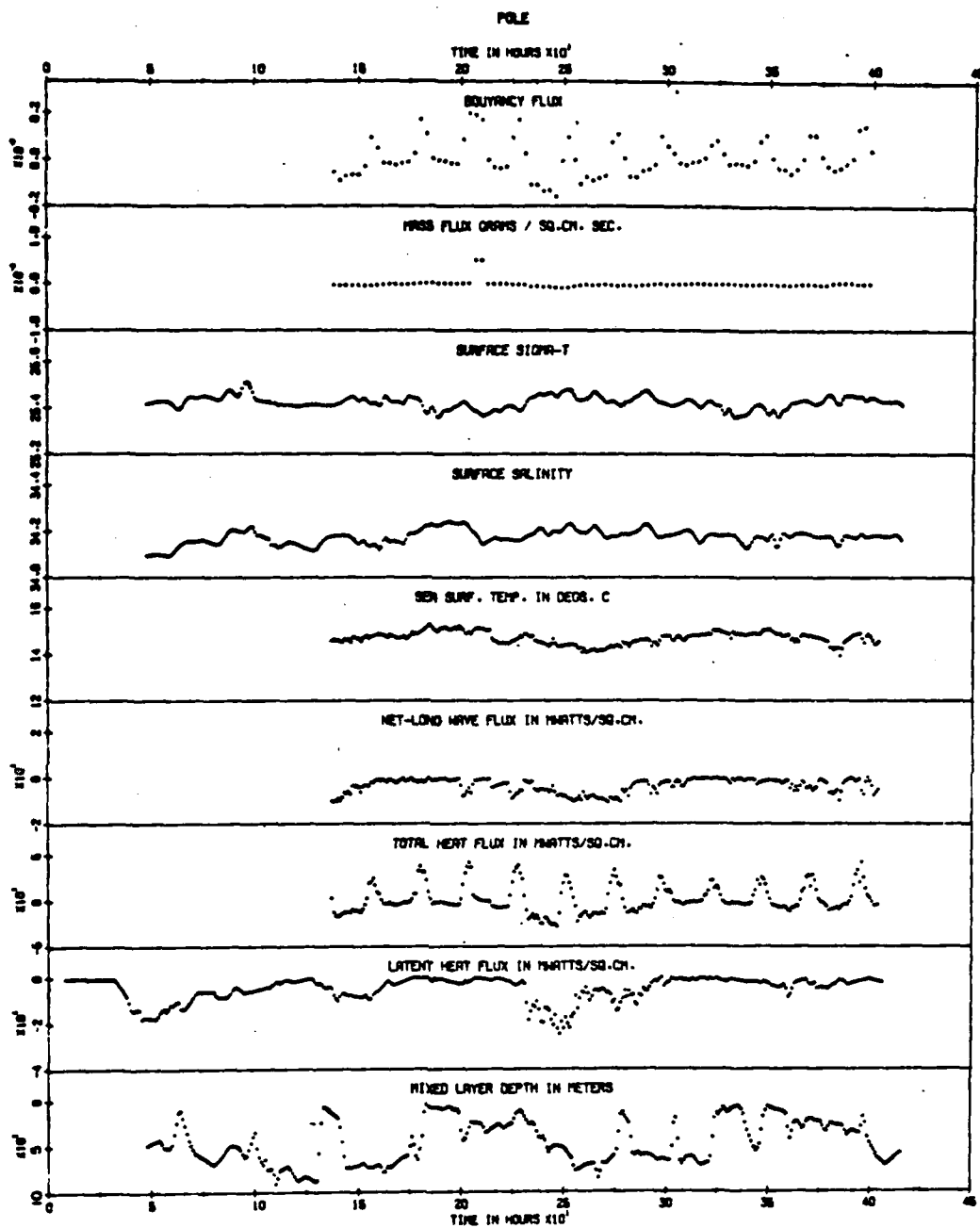
Figure 17. Interpolated hourly values of mass and buoyancy fluxes, surface salinity, sea surface temperature, surface sigma-t, and the various components of the heat flux involved in the determination of the buoyancy flux. (Simpson and Paulson 1977)

51
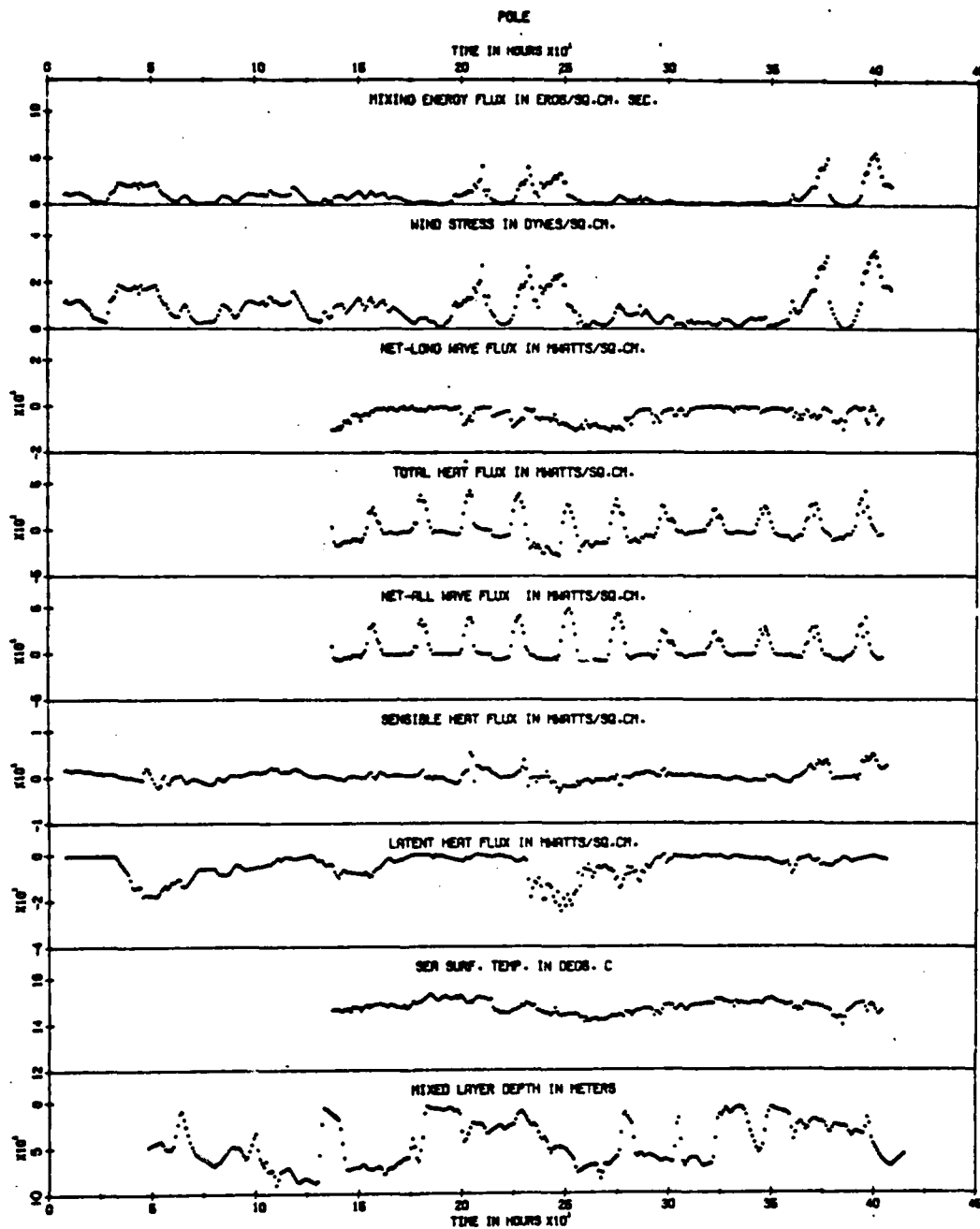
Figure 18. Interpolated hourly values of the various components of the surface momentum and heat balance are shown. (Simpson and Paulson 1977)

52
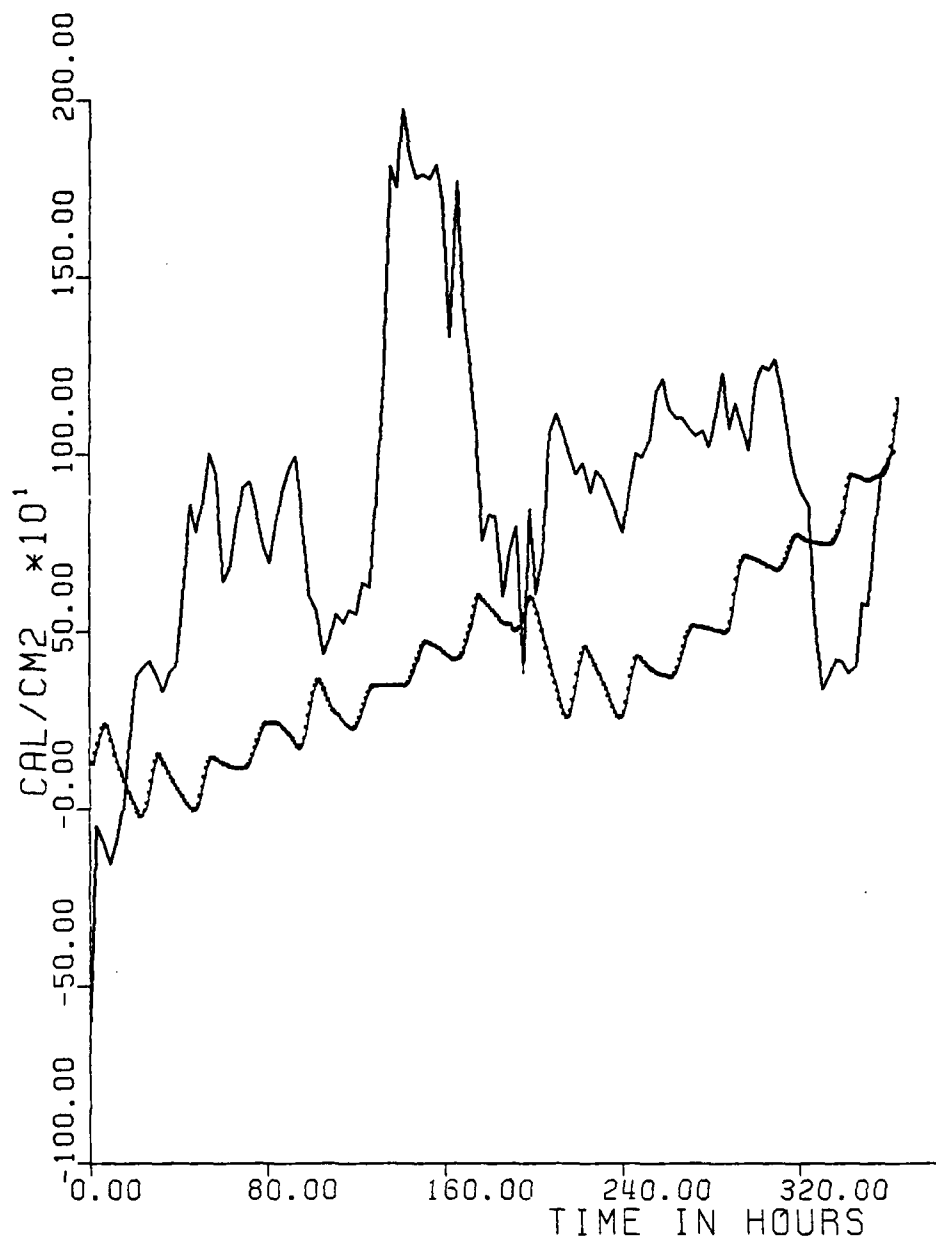
Figure 19.   The observed changes in heat content in the upper
            40 meters (solid line). Model computed accumulated
            surface heat flux (dotted line). The origin of the
            abscissa is 0000 hour (local) 30 January 74.

53
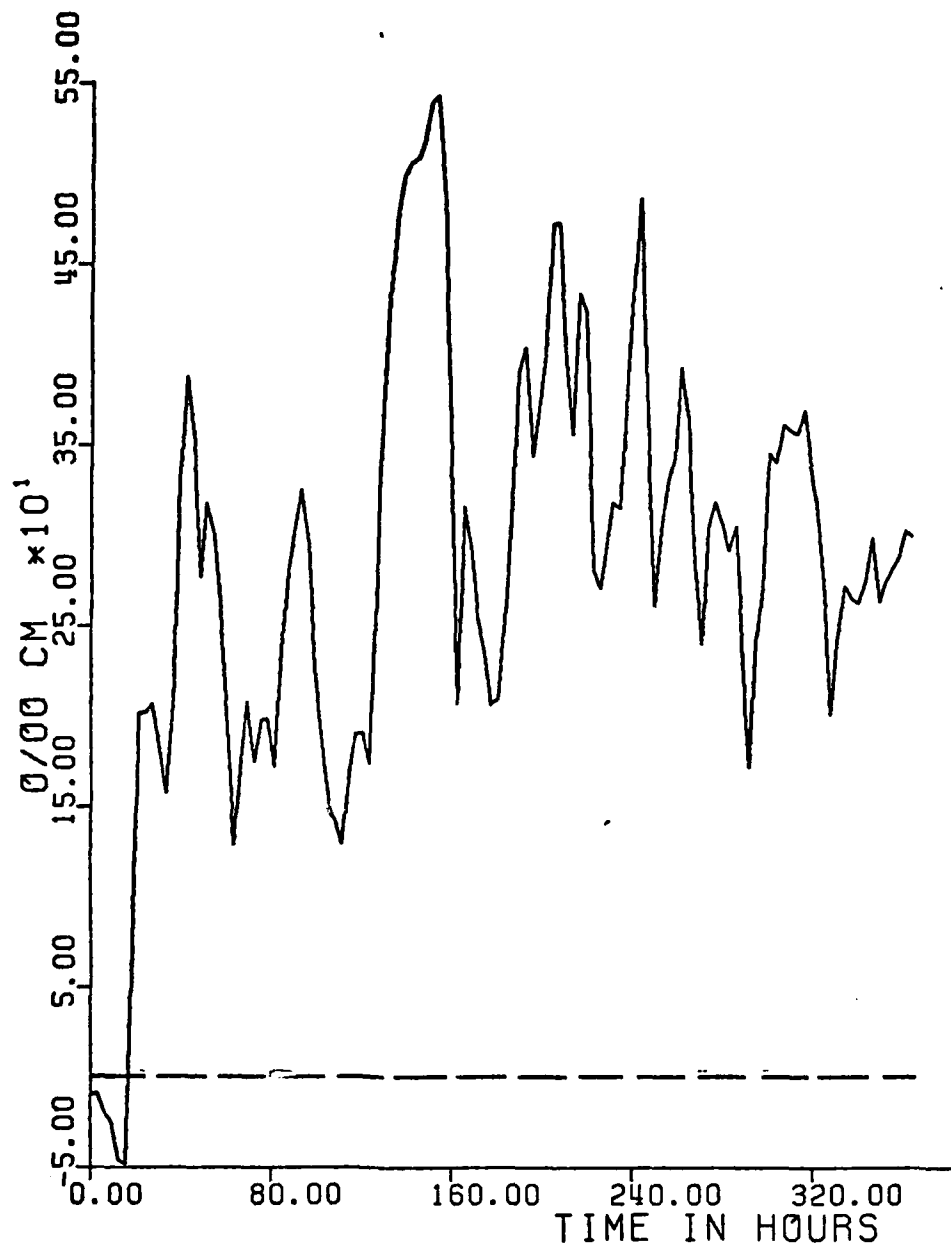
Figure 20. The observed changes in salt content in upper 40 meters (solid line). Model-computed accumulated surface salinity flux $(\overline{S'w'}_0)$, dashed line, which is negligible in comparison with the observed changes in salt content. The origin of the abscissa is 0000 hour (local) 30 January 74.

54
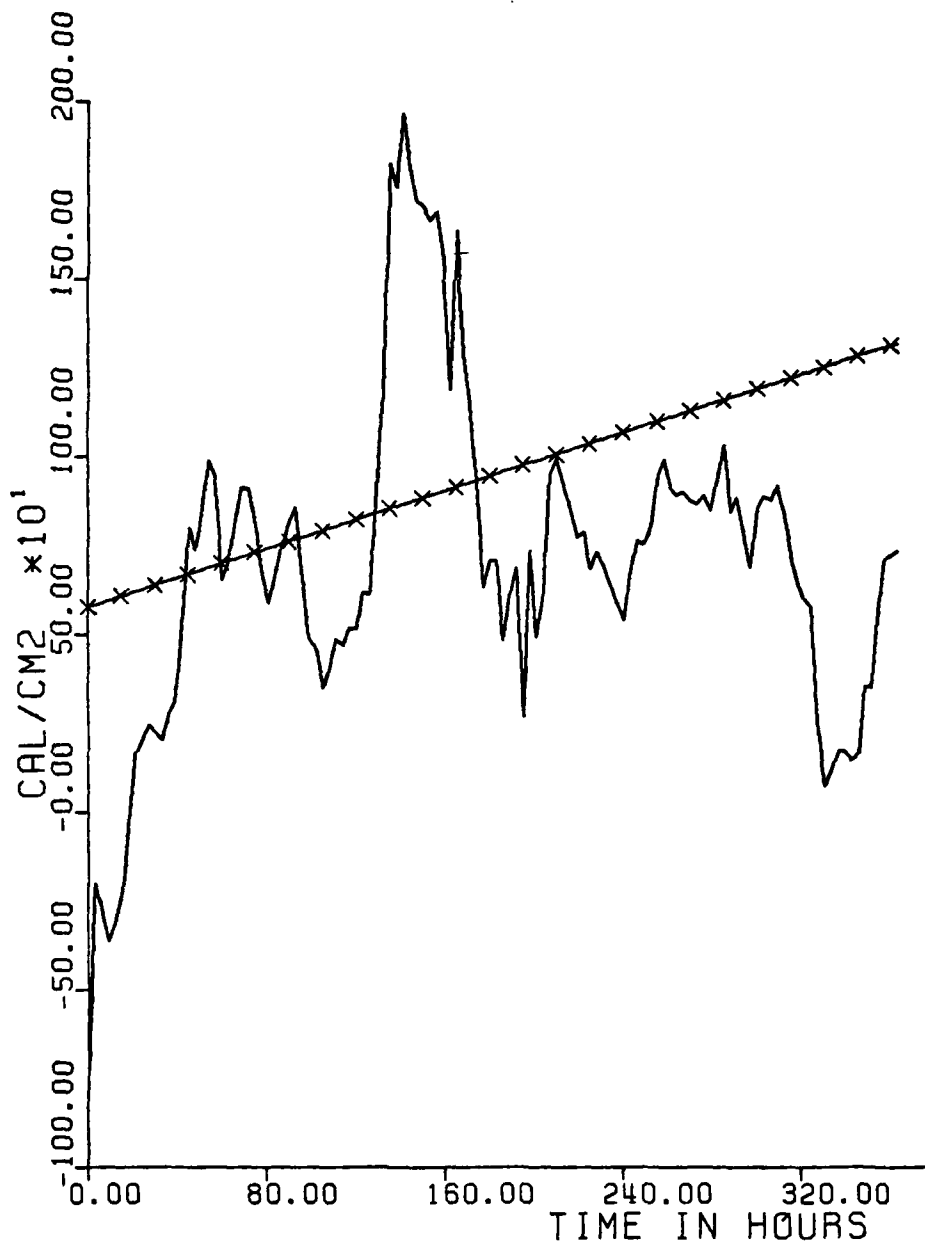
Figure 21. Advection of heat (solid line) determined by subtracting the accumulated heat flux from the change in heat content (Figure 21). Least squares fit to data resulted in a slope 2.0 cal cm^{-2} hour^{-1}.

55
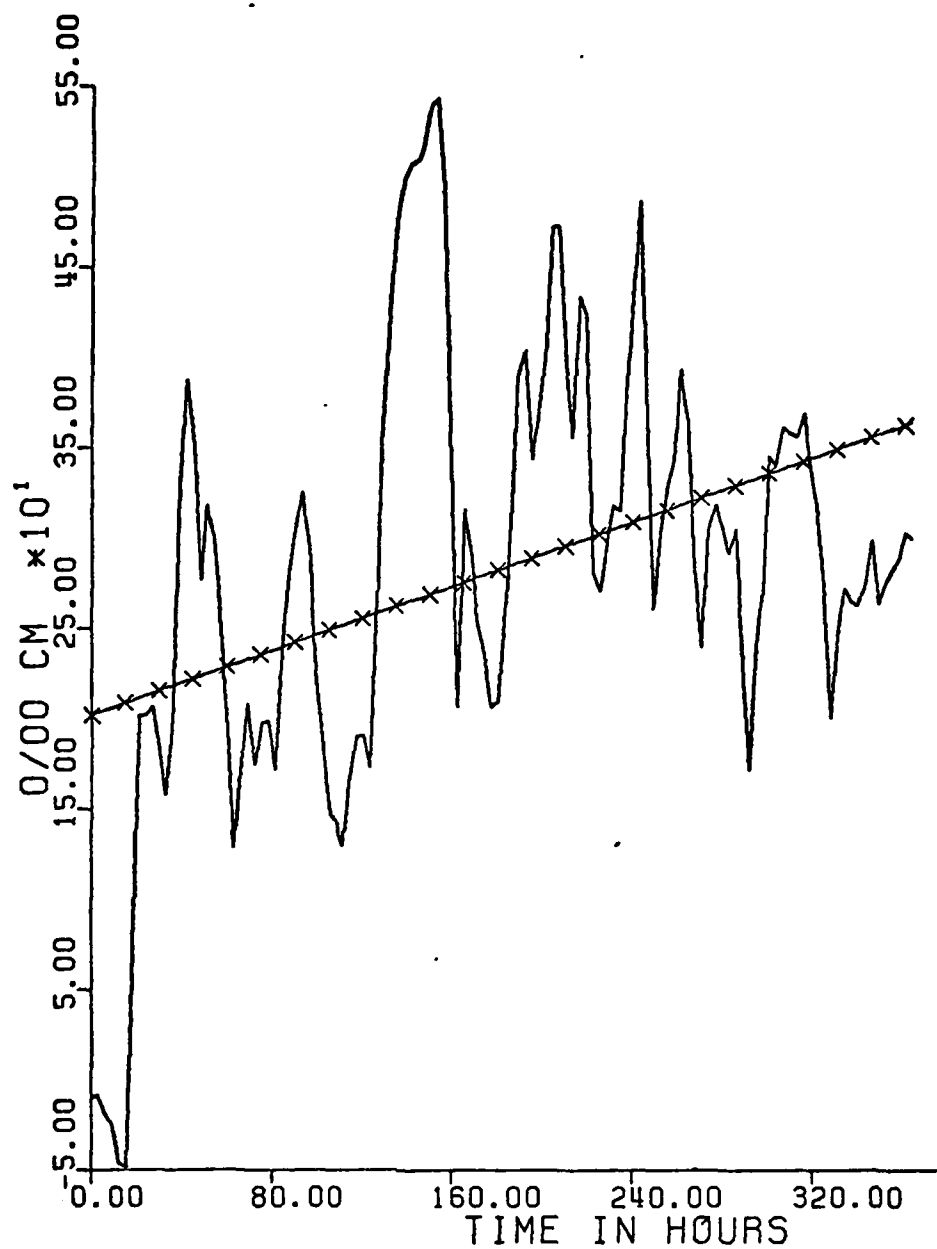
Figure 22. Advection of salt (solid line) determined by subtracting the accumulated surface salinity flux from the changes in salt content (Figure 20). Least square fit to data resulted in a slope 0.45 0/00 cm hour^{-1}.

56
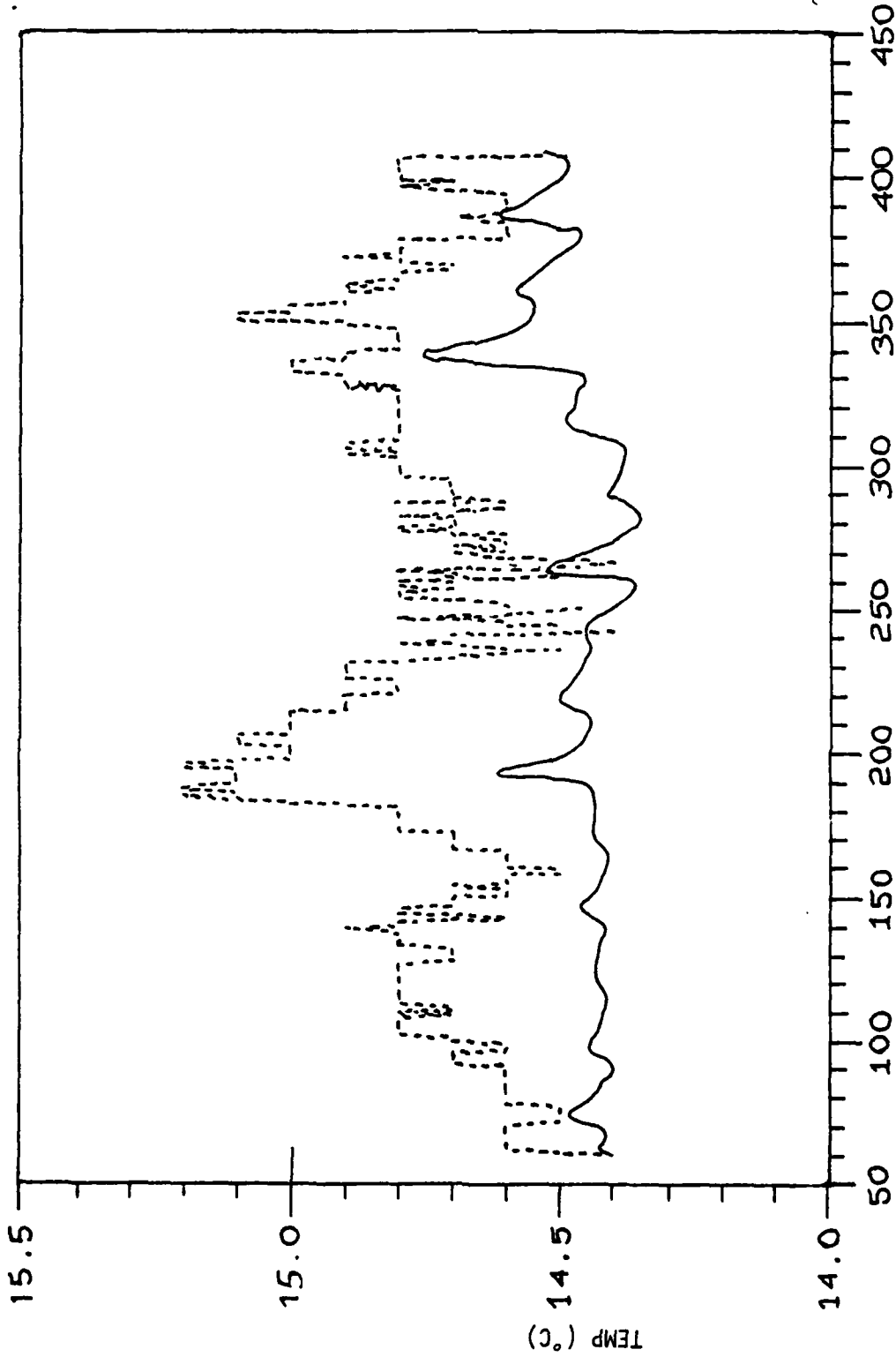
Figure 23. Comparison of model computed mixed layer temperature (solid line) with observed for sea surface temperature (dotted line). Model computed mixed layer temperature has been offset slightly for the comparison. The origin of the abscissa is 1200 GMT 30 January 1974.

57
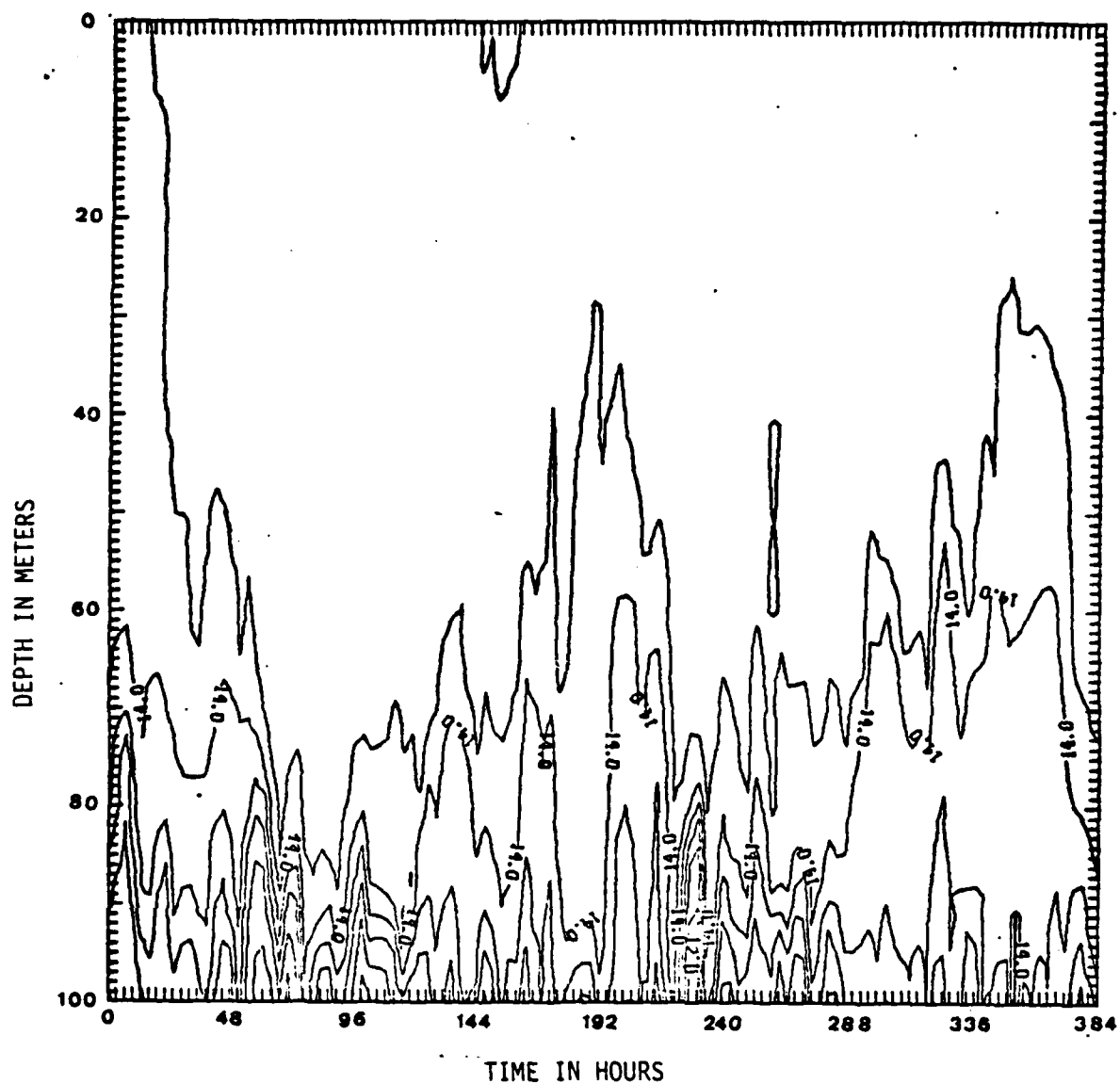
Figure 24. Isotherm distribution for the period 30 Jan 74 through 14 Feb 74. The contour interval is 0.5°C.

58
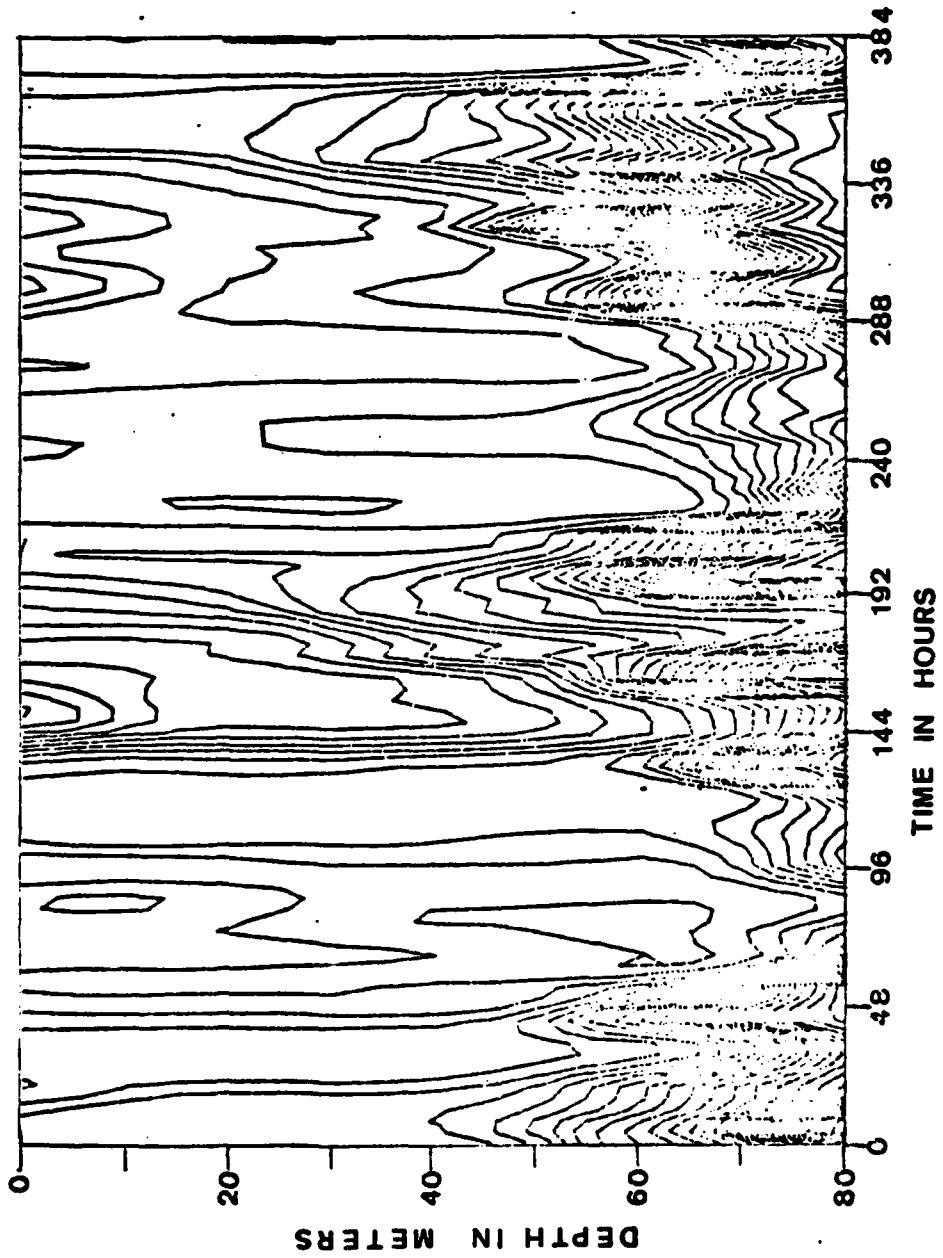
Figure 25.   Isotherm distribution, smoothed twice, for period 30 Jan 74 through 14 Feb 74.   The contour interval is 0.05°C.

59
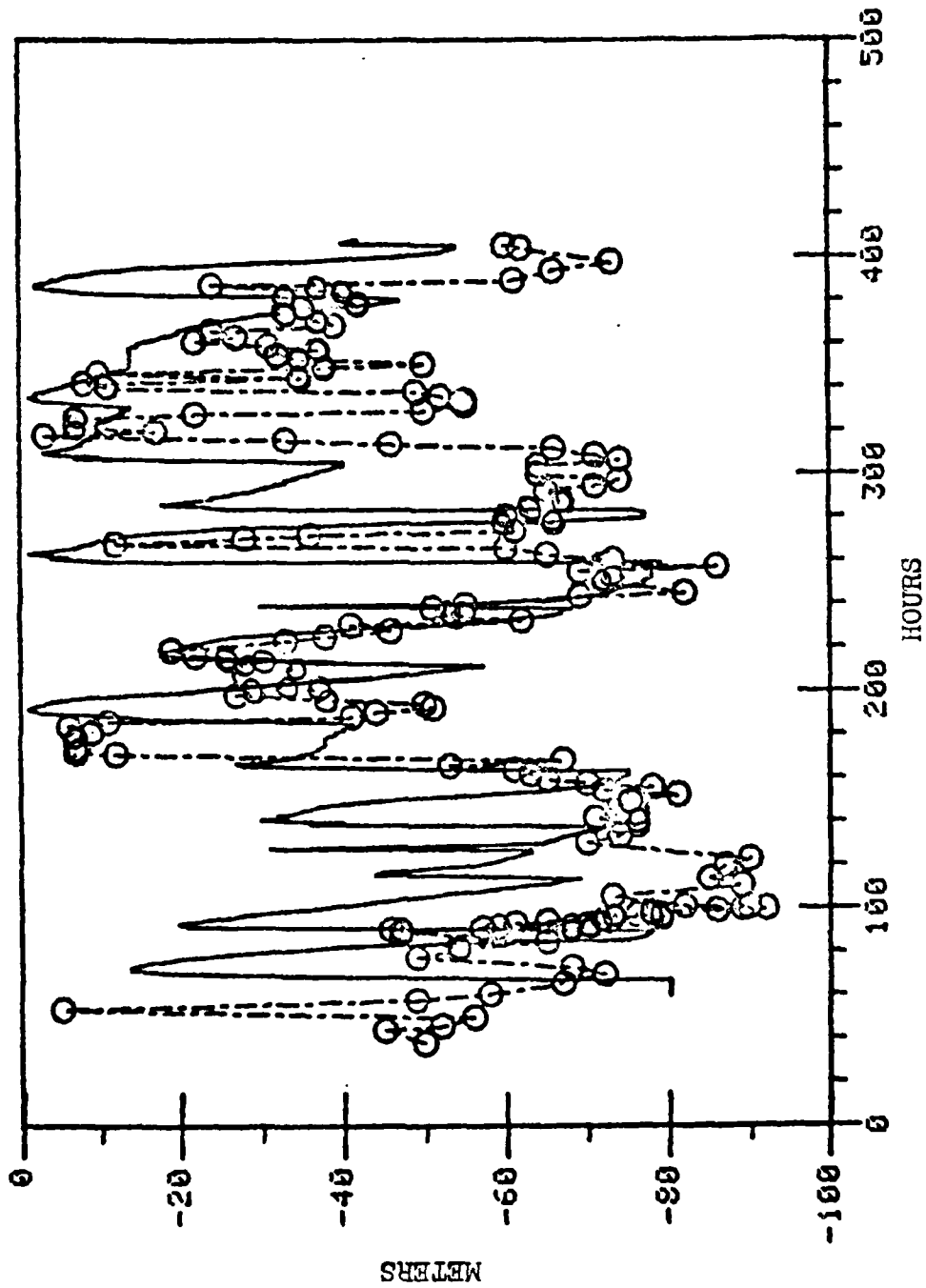
Figure 26. The dashed line with the symbol (0) is the observed mixed layer depth, $h_0(t)$. The solid line is the model computed turbulent boundary layer depth, $h(t)$. The origin of the abscissa is 1000 GMT 28 January 1974.

60
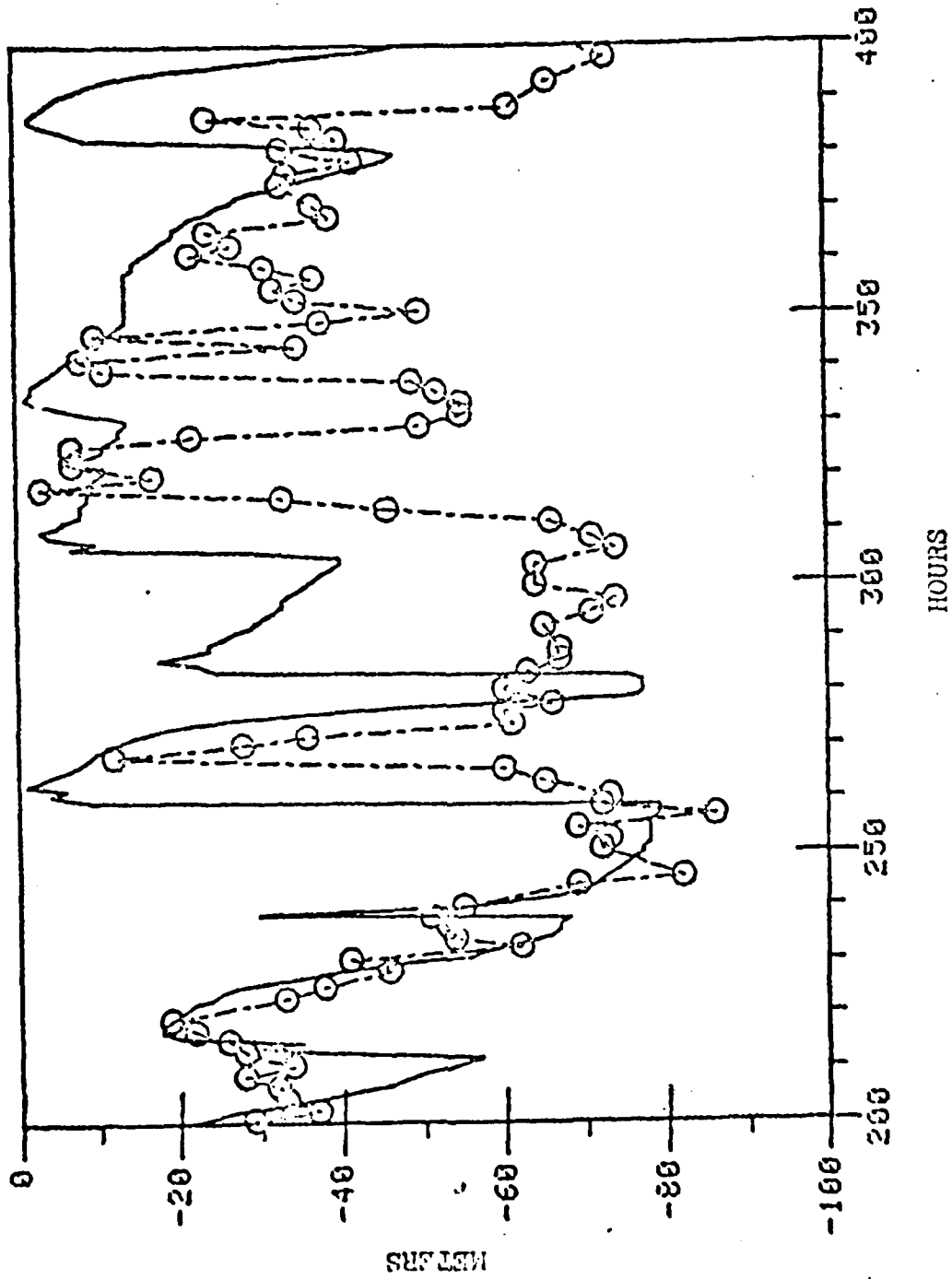
Figure 27. The dashed line with the symbol (0) is the observed mixed layer depth, $h_0(t)$. The solid line is model computed turbulent boundary layer depth, $h(t)$.

61
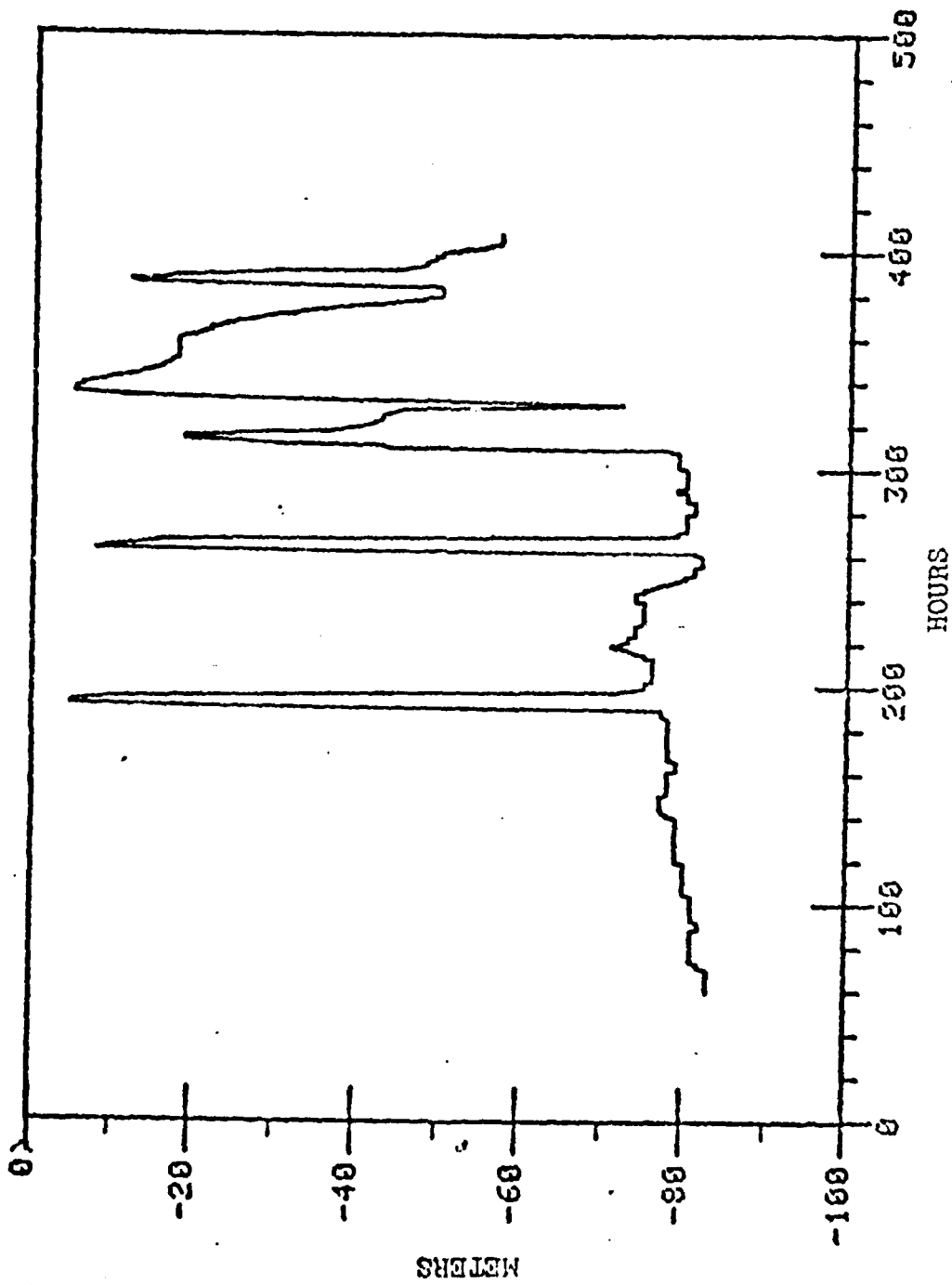
Figure 28. Model computed mixed layer depth, $h_1(t)$. The origin of the abscissa is 1000 GMT 28 January 1974.

62
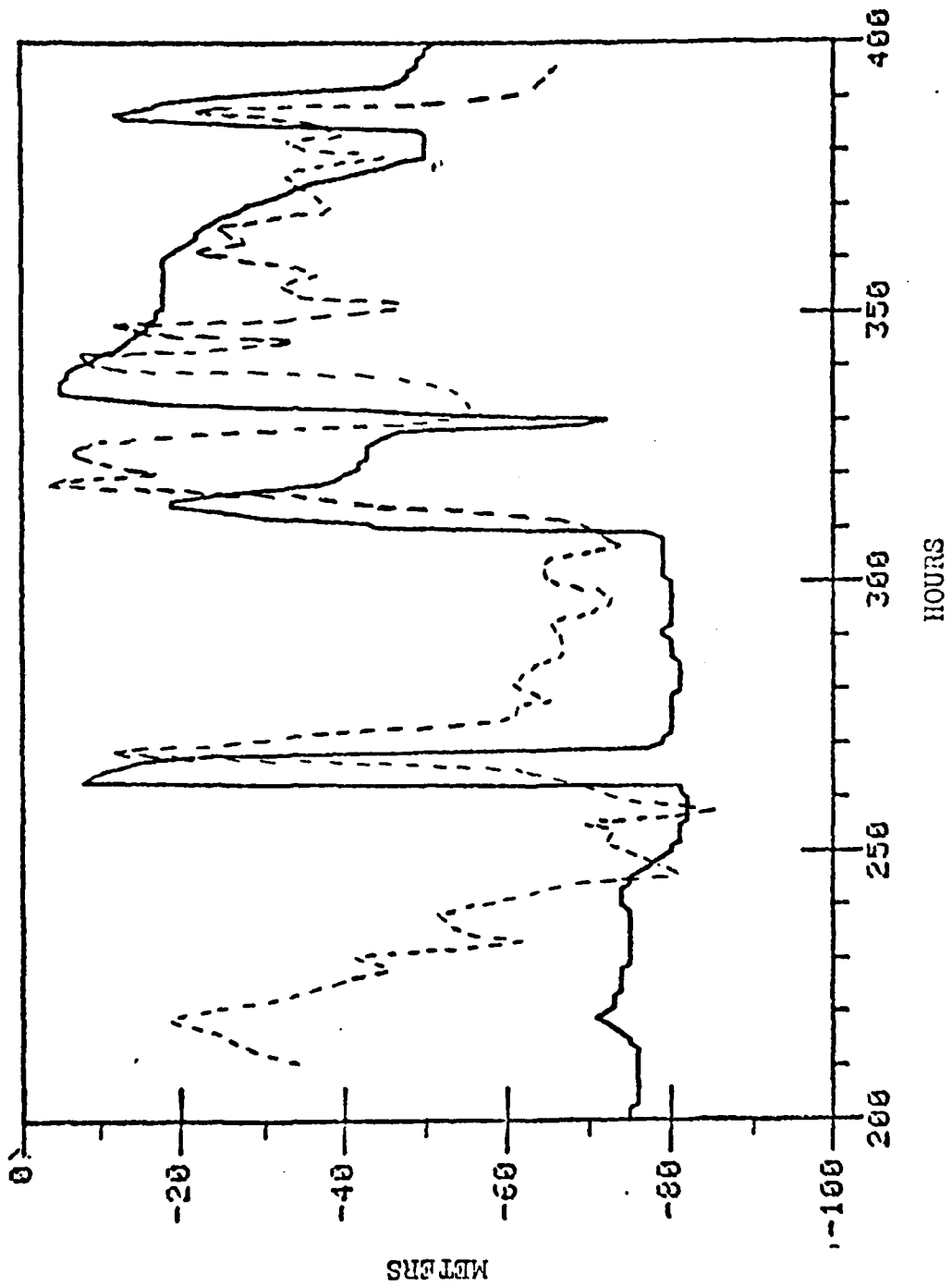
Figure 29. Model computed mixed layer depth (solid line), $h_1(t)$. Observed mixed layer depth (dashed line), $h_0(t)$.

63
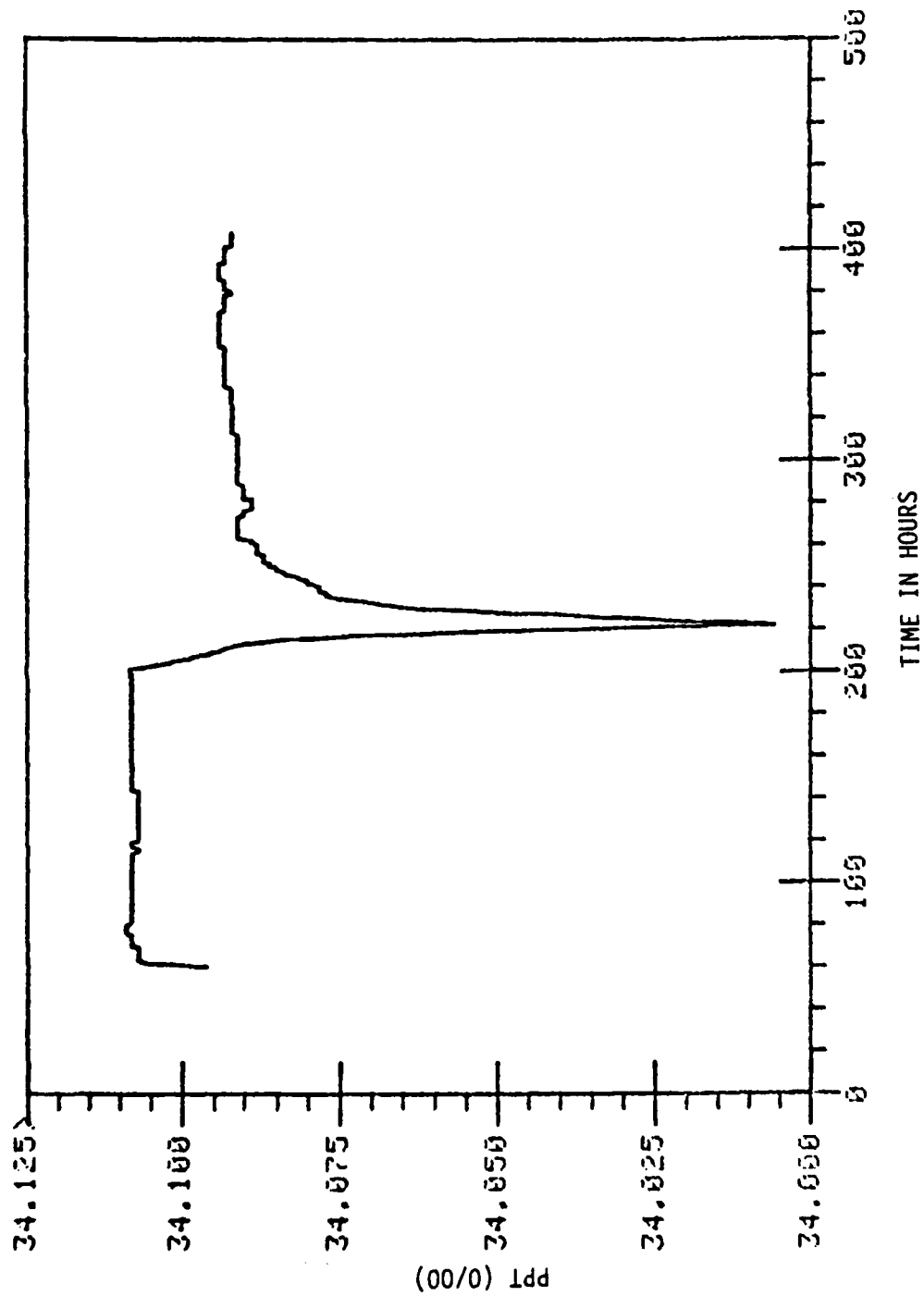
Figure 30. Model computed hourly values of surface salinity with a hypothetical amount of precipitation (5×10^{-5} gm cm^{-2} sec^{-1}), starting at time = 220.

64
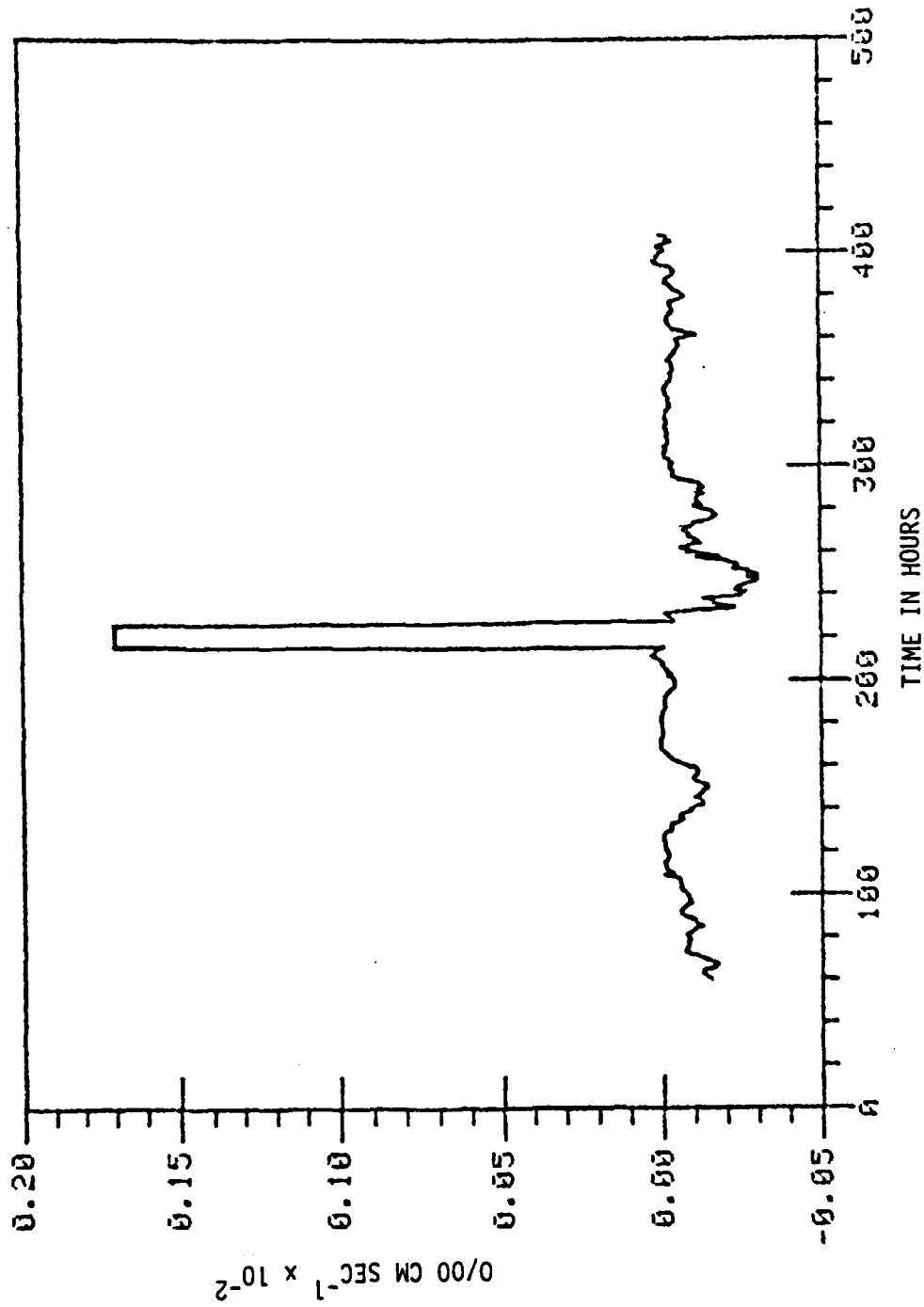
Figure 31. Model computed hourly values of salinity flux ($\overline{S'w'} = (P-E)S_0$) with hypothetical precipitation (5×10^{-5} gm cm^{-2} sec^{-1}), starting at time = 220.

65
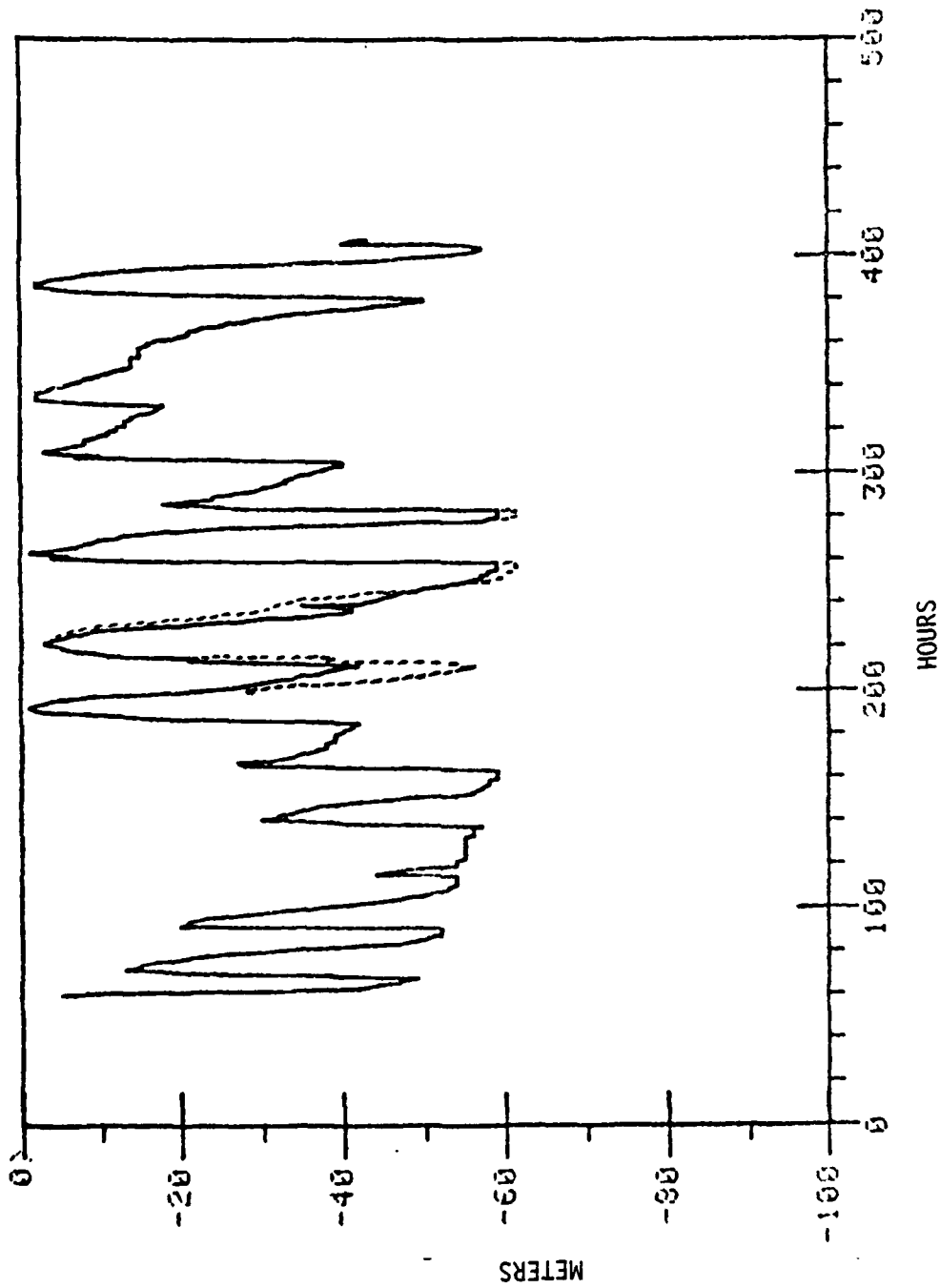
Figure 32. The dashed line shows the model computed mixed layer depth, h(t), without considering the effect of precipitation. The solid line shows a decrease in the model computed mixed layer depth as a result of including the precipitation (5×10^{-5} gm cm^{-2} sec^{-1}).

66

LIST OF REFERENCES

Alexander, R.C., and J.W. Kim, 1976: Diagnostic Model Study of Mixed Layer Depth in the Summer North Pacific, J. Phys. Oceanogr., 6, 293-298.

Barnett, T.P., 1976: Large Scale Variations of the Temperature Field in the North Pacific Ocean, Naval Research Reviews, March, 36-51.

Camp, N.T., 1976: The Role of Strong Atmospheric Forcing Events in the Modification of the Upper Ocean Thermal Structure During the Cooling Season, Ph.D dissertation, Naval Postgraduate School, 175 pp.

Davis, R., T.B. Barnett and C.S. Cox, 1978: Variability of Near - Surface Currents Observed During the POLE Experiment J. Phy. Oceanogr., 8, 290-301.

DeSzoeke, R.A., and P.B. Rhines, 1976: Asynptotic Regimes in the Mixed Layer Deepening, J. Mar. Res., 34, 111-116.

Ekman, V.W., 1905: On the Influence of the Earth's Rotation on Ocean Currents, ARK. Mat. Astron. Fysik., 2, 1-53.

Elsberry, R., T. Fraim, and R. Trapnell, Jr., 1976: A Mixed Layer Model of the Ocean Thermal Response to Hurricanes, J. Geophys. Res., 8, 1153-1162.

Elsberry, R.L., and N.T. Camp, 1978: Ocean Thermal Response to Strong Atmospheric Forcing, 1, Characteristics of Forcing Events, J. Phy. Oceanogr., 8, 206-214.

Elsberry, R.L., and S.D. Raney, 1978: Sea Surface Temperature Response to Variations in Atmospheric Wind Forcing, J. Phys. Oceanogr., 8, 881-887.

Garwood, R.W., and D. Halpern, 1976: Numerical Simulation of Long-Period Response of the Upper Ocean to Diurnal-Period Fluctuation of Wind-Stress and Surface Buoyancy Flux, Bull. Am. Meteorol. Soc., 57, 134.

Garwood, R.W., 1976: A General Model of the Ocean Mixed Layer Using a Two Component Turbulent Kinetic Energy Budget with Mean Turbulent Field Closure, NOAA-TR-ERL-384, 95 pp., NTIS, Dept. of Commerce, Springfield, Va.

Garwood, R.W., Jr., 1977: An Oceanic Mixed Layer Model Capable of Simulating Cyclic States, J. Phys. Oceanogr., 7, 455-468.

Husby, D.M., and G.R. Seckel, 1978: Large Scale Air-Sea Interactions at Ocean Weather Station V, 1951-1971, NOAA Tech. Rep. NMFS SSRF-696, 44 pp.

Jones, I.S.F., and B.C. Kenney, 1977: The Scaling of the Velocity Fluctuations in the Surface Mixed Layer, J. Geophys. Res., 82, 1392-1396.

Kim, J., 1976: A Generalized Bulk Model of the Oceanic Mixed Layer, J. Phys. Oceanogr., 6, 686-695.

Kraus, E.B., and C. Rooth, 1961: Temperature and Steady State Vertical Heat Flux in the Ocean Surface Layers, Tellus, 13, 231-239.

Kraus, E.B., and J.S. Turner, 1967: A One-Dimensional Model of the Seasonal Thermocline, Part II, Tellus, 19, 98-105.

Kroll, J., 1975: The Propagation of the Wind-Generated Inertial Oscillations from the Surface into the Deep Ocean, J. Mar. Res., 33, 15-51.

Laevastu, T., 1960: Factors Affecting the Temperature of Surface Layer of the Sea, Soc. Scient. Femica. Comment. Physico-Mathem., 25(1), 1-136.

List, R.J., 1958: Smithsonian Meteorlogical Tables, Smithsonian Institution (Washington), 527 pp.

Mellor, G.L., and P.A. Durbin, 1975: The Structure and Dynamics of the Ocean Surface Mixed Layer, J. Phys. Oceanogr., 5, 718-728.

Miller, J.R., 1976: The Salinity Effects in a Mixed Layer Ocean Model, J. Phys. Oceanogr., 6, 39-35.

Niiler, P.P., 1975: Deepening of the Wind Mixed Layer, J. Mar. Res., 33, 405-422.

Norpac Atlas, 1960: Oceanic Observations of the Pacific: 1955, prepared by the NORPAC Committee, University of California Press, 10.

Paulus, R.A., 1978: Salinity Effects in an Oceanic Mixed Layer Model, M.S. Thesis, Naval Postgraduate School, Monterey, Ca., 77 pp.

Pollard, R.T., P.B. Rhines, and R.O.R.Y. Thompson, 1973: The Deepening of the Wind-Mixed Layer, J. Geophys. Fluid Dyn., 3, 381-404.

Pollard, R.T., and S. Tarbel, 1975: A Compilation of Moored Current Meters and Wind Observations, Vol. VIII (1970 array experiment), Woods Hole Oceanographic Inst., Ref 75-7.

Pollard, R.T., 1977: Observation and Models of the Structure of the Upper Ocean, Modeling and Prediction of the Upper Layers of the Ocean, Edited by E.B. Kraus, Pergamon Press, 102-117.

68

Powell, T.M., P.J. Richerson, T.M. Dillon, B.A. Agree, B. Dozier, D.A. Godden, and L.O. Myrup, 1975: Spatial Scales of Current Speed and Phytoplankton Biomass Fluctuations in Lake Tahoe, Science, 189, 1088-1090.

Price, J.F., 1977: Observation and Simulation of Storm Driven Mixed Layer Deepening, Ph.D. Thesis, University of Miami, 192 pp.

Roden, G.I., 1974: Thermohaline Structures, Fronts and Air-Sea Energy Exchanges of the Trade Winds East of Hawaii, J. Phys. Oceanogr., v 4, 168-182.

Seckel, G.R., and F.H. Beaudry, 1973: The Radiation from Sun and Sky over the North Pacific Ocean, (Abstract O-33), EOS, TRANS. AM. Geophys. Union, 54, 1114.

Simpson, J.J., and Paulson, C.A., 1977: Mixed Layer Observations During the NORPAX POLE Experiment: a data report, Oregon State University, Data Report 66, Reference 77-5, 167.

Simpson, J.J., 1977: Small Scale Temperature Structure of the Upper Ocean, Ph.D. dissertation, Oregon State University, 148 pp.

Simpson, J.J., and Paulson, C.A., 1979: Observations of Upper Ocean Temperature and Salinity Structure During the POLE Experiment, J. Phys. Oceanogr., 9, 869-884.

Stevenson, J.W., 1979: On the Effect of Dissipation on Seasonal Thermocline Models, J. Phys. Oceanogr., 9, 57-64.

Tabata, S., 1964: A Study of the Main Physical Factors Governing the Oceanographic Conditions of Station P in the Northeast Pacific Ocean, Ph.D. Thesis, University of Tokyo, 264 pp.

Thompson, R., 1976: Climatolgical Numerical Models of the Surface Mixed Layer of the Ocean, J. Phys. Oceanogr., 6, 496-503.

Wyrtki, K., 1965: The Average Annual Heat Balance of the North Pacific Ocean and in Relation to Ocean Circulation, J. Geophys. Res., 70, 4547-4559.

Yun, J.Y., 1978: The Frequency Dependent Response and Asymptotic Properties of the Turbulent Mixing in the Upper Ocean, M.S. Thesis, Naval Postgraduate School, Monterey, Ca., 87 pp.

Zeman, O., and H. Tennekes, 1975: A Self-Contained Model for the Pressure Terms in the Turbulent Stress Equation of the Neutral Atmospheric Boundary Layer, J. Atmos. Sci., 32, 1808-1813.

INITIAL DISTRIBUTION LIST

		No. Copies
1.	Defense Technical Information Center Cameron Station Alexandria, VA 22314	2
2.	Library, Code 0142 Naval Postgraduate School Monterey, CA 93940	2
3.	Chairman, Code 68 Department of Oceanography Naval Postgraduate School Monterey, CA 93940	1
4.	Chairman, Code 63 Department of Meteorology Naval Postgraduate School Monterey, CA 93940	1
5.	Professor R.W. Garwood, Code 68Gd Department of Oceanography Naval Postgraduate School Monterey, CA 93940	2
6.	Lieutenant Ricky E. Shook HELANTISUBRON ELEVEN NAS Jacksonville, FL 09954	2
7.	Professor R.L. Elsberry, Code 63Es Department of Meteorology Naval Postgraduate School Monterey, CA 93940	1
8.	Director Naval Oceanography Division Navy Observatory 34th and Massachusetts Avenue NW Washington, D.C. 20390	1
9.	Commander Naval Oceanography Command NSTL Station Bay St. Louis, MS 39529	1

10. Commanding Officer   1
    Naval Oceanographic Office
    NSTL Station
    Bay St. Louis, MS 39529

11. Commanding Officer   1
    Fleet Numerical Oceanography Center
    Monterey, CA 93940

12. Commanding Officer   1
    Naval Environmental Prediction Research Facility
    Monterey, CA 93940

13. Commanding Officer   1
    Naval Ocean Research and Development Activity
    NSTL Station
    Bay St. Louis, MS 39529

14. Office of Naval Research (Code 480)   1
    Naval Ocean Research and Development Activity
    NSTL Station
    Bay St. Louis, MS 39529

15. Scientific Liaison Office   1
    Office of Naval Research
    Scripps Institution of Oceanography
    La Jolla, CA 92037

16. Library   1
    Scripps Institution of Oceanography
    P.O. Box 2367
    La Jolla, CA 92037

17. Library   1
    Department of Oceanography
    University of Washington
    Seattle, WA 98105

18. Library   1
    CICESE
    P.O. Box 4803
    San Ysidro, CA 92073

19. Library   1
    School of Oceanography
    Oregon State University
    Corvallis, OR 97331

20. Commander   1
    Oceanographic Systems Pacific
    Box 1390
    Pearl Harbor, HI 96860

21. Chief, Ocean Services Division   1
    National Oceanic and Atmospheric Administration
    8060 Thirteenth Street
    Silver Springs, MD 20910

22. Chairman, Oceanography Department   1
    U.S. Naval Academy
    Annapolis, MD 21402

FILMED

—8